ADVANCED ENERGY MATERIALS
www.advenergymat.de

Lithium Manganese Spinel Cathodes for Lithium-Ion Batteries

*Yimeng Huang, Yanhao Dong, Sa Li, Jinhyuk Lee, Chao Wang, Zhi Zhu, Weijiang Xue, Yao Li, and Ju Li**

Spinel $LiMn_2O_4$, whose electrochemical activity was first reported by Prof. John B. Goodenough's group at Oxford in 1983, is an important cathode material for lithium-ion batteries that has attracted continuous academic and industrial interest. It is cheap and environmentally friendly, and has excellent rate performance with 3D Li^+ diffusion channels. However, it suffers from severe degradation, especially under extreme voltages and during high-temperature operation. Here, the current understanding and future trends of the spinel cathode and its derivatives with cubic lattice symmetry ($LiNi_{0.5}Mn_{1.5}O_4$ that shows high-voltage stability, and Li-rich spinels that show reversible hybrid anion- and cation-redox activities) are discussed. Special attention is given to the degradation mechanisms and further development of spinel cathodes, as well as concepts of utilizing the cubic spinel structure to stabilize high-capacity layered cathodes and as robust framework for high-rate electrodes. "Good spinel" surface phases like $LiNi_{0.5}Mn_{1.5}O_4$ are distinguished from "bad spinel" surface phases like Mn_3O_4.

1. Introduction

Lithium-ion batteries (LIBs) have enjoyed great success in portable electronics and electric vehicles, and show considerable prospects in grid level energy storage. Such development dramatically accelerates the progress of modern civilization and is acknowledged by the 2019 Nobel Prize in Chemistry awarded to John B. Goodenough, M. Stanley Whittingham, and Akira Yoshino.[1] Among many other milestones that contributed to the huge success of LIBs is the development of three families of cathode materials (layered structure $LiCoO_2$,[2] spinel structure $LiMn_2O_4$,[3] and olivine structure $LiFePO_4$[4]) pioneered by Goodenough and co-workers. This review article shall focus on manganese spinel cathode $LiMn_2O_4$ and its derivatives, with cubic lattice symmetry on average.

The discovery of $LiMn_2O_4$ for battery applications came from the quest to find an inexpensive oxide as the cathode material.[5] In 1981, Hunter[6] first reported the conversion of spinel $LiMn_2O_4$ into a new form of manganese dioxide called λ-MnO_2 by chemical delithiation in aqueous acidic solutions. The λ-MnO_2 preserves the $[B_2]O_4$ framework of $A[B_2]O_4$ spinel and turns out to be the end product of $LiMn_2O_4$ after electrochemical delithiation. After early investigations of electrochemical lithiation of Fe_3O_4 spinel,[7] Thackeray et al. reported electrochemical lithiation[3a] and delithiation[3b] of $LiMn_2O_4$ spinel in 1983 and 1984, respectively, which boosted research interest in this family of cathodes with good thermal stability.[8] Further investigations of complex phase diagrams and versatile structure/chemistry of Mn-based materials[9] as well as efforts to optimize the electrochemical properties (especially on cycling)[10] led to the discovery and development of high-voltage spinel cathodes (e.g., $LiNi_{0.5}Mn_{1.5}O_4$[11]), high-capacity layered Li-/Mn-rich cathodes (e.g., Li_2MnO_3 and $xLiNi_{1/3}Co_{1/3}Mn_{1/3}O_2 \cdot (1-x)Li_2MnO_3$[12]), and other advanced cathode materials/composites.[13] The major milestones of the development of $LiMn_2O_4$ and its derivatives are briefly summarized in the flow chart in **Figure 1**. To date, even though $LiMn_2O_4$ has smaller capacity and energy density compared to the later developed layered $LiNi_{1-x-y}Co_xMn_yO_2$ (NCM), $LiNi_{1-x-y}Co_xAl_yO_2$ (NCA), Li-/Mn-rich cathodes, and $LiCoO_2$ (see comparison of different cathode materials in **Table 1**), it is cost-effective, nontoxic, and environmentally friendly (cobalt-free, with abundant nontoxic manganese) and has a more robust crystal structure with fast diffusion kinetics, so it is commonly blended with layered cathodes to reduce cost, increase structural and thermal stability, and improve rate performance.[14] High-voltage spinel $LiNi_{0.5}Mn_{1.5}O_4$ has

Y. Huang, Prof. J. Li
Department of Materials Science and Engineering
Massachusetts Institute of Technology
Cambridge, MA 02139, USA
E-mail: liju@mit.edu

Dr. Y. Dong, Prof. J. Lee, Dr. C. Wang, Dr. Z. Zhu, Dr. W. Xue, Dr. Y. Li, Prof. J. Li
Department of Nuclear Science and Engineering
Massachusetts Institute of Technology
Cambridge, MA 02139, USA

Prof. S. Li
Institute of New Energy for Vehicles
School of Materials Science & Engineering
Tongji University
Shanghai 201804, China

Prof. J. Lee
Department of Mining and Materials Engineering
McGill University
Montreal, Quebec H3A 0C5, Canada

Dr. Y. Li
State Key Laboratory of Metal Matrix Composites
Shanghai Jiao Tong University
Shanghai 200240, China

The ORCID identification number(s) for the author(s) of this article can be found under https://doi.org/10.1002/aenm.202000997.

DOI: 10.1002/aenm.202000997

 © 2020 WILEY-VCH Verlag GmbH & Co. KGaA, Weinheim

promising energy density due to its high operating voltage at ≈4.7 V versus Li^+/Li. Also, the spinel structure is closely related to the layered and rocksalt structures of many LIB cathodes, and spinel-like structures can often be observed at the surface of degraded cathodes. And, just like Li substitution of transition metals (TM) in layered compounds leads to Li-rich cathodes with higher capacity due to the participation of oxygen redox, one may also create Li-rich spinels with reversible and/or irreversible hybrid anion- and cation-redox (HACR) activities.

Here, we would like to make a distinction between "bad spinel" structures like the Co_3O_4 phase, where Li^+ diffusion channels are all blocked as both tetrahedral and octahedral sites are occupied by Co, and "good spinel" structures like $LiMn_2O_4$ and $LiNi_{0.5}Mn_{1.5}O_4$ where there are percolating 3D Li^+ diffusion channels. In this review, we are mostly concerned with the latter, although on the surfaces of some layered compounds, "bad spinel" can also form, greatly increasing the impedance. "Good spinel" surface phases, on the other hand, do not necessarily degrade the rate performance and can actually improve it.[17]

Past understanding and lessons learned from spinel cathodes could provide valuable insights and implications for future development of LIB cathodes in general. This review is organized as follows. Section 2 describes the fundamentals of spinel cathodes and its relation to layered and rocksalt lattice structures. Section 3 summarizes the understandings of their degradation mechanisms. Section 4 discusses degradation mitigation and future development strategies, including bulk doping, controlling dopant distribution (e.g., cation ordering and surface doping), coating, and development of novel liquid and solid electrolytes. Section 5 discusses the stability of the spinel structure, summarizes the observations of spinel-like surface structures in degraded layered cathodes, and discusses the integration of the spinel structure into the layered cathodes as structural stabilizer. Section 6 discusses the origin of fast kinetics in the spinel structure and the potential application of utilizing the spinel structure to design novel high-rate cathodes. Section 7 provides a conclusion with a summary of future directions for spinel cathodes.

2. Fundamentals of $LiMn_2O_4$ and Its Derivatives

$LiMn_2O_4$ has a cubic spinel structure $A[B_2]O_4$ under the space group $Fd\overline{3}m$, where O anions form face-centered cubic (FCC) array at 32e (Wyckoff position), B-site Mn cations fill in 1/2 of the octahedral sites at 16d, and A-site Li cations fill in 1/8 of the tetrahedral sites at 8a. The 3D $[B_2]O_4$ array is formed by edge-sharing MnO_6 octahedra (**Figure 2**a), which offers a strongly bonded network for 3D Li^+ diffusion via the empty octahedral sites at 16c (Figure 2b). The LiO_4 tetrahedra centered at 8a sites are corner-shared with MnO_6 octahedra centered at 16d and face-shared with empty octahedra centered at 16c, and Li hops from 8a → 16c → 8a. This spinel structure (**Figure 3**, bottom panel) is closely related to the layered $Li(TM)O_2$ structure (Figure 3, top panel; which can also be viewed as an ordered rocksalt structure), both with the same FCC anion sublattice, but with different cation sublattice (octahedral + tetrahedral) occupations. The layered compound $Li(TM)O_2$ has a planar Li–TM–Li–TM cation concentration wave, with Li/(Li+TM) of 100% and 0% in the alternating layers, all at octahedral sites, with an average TM valence of 3+. By contrast, the cubic spinel $Li(TM)_2O_4$ has Li/(Li+TM) occupation of 66.7% in one layer (octahedral + tetrahedral) and 0% in the other layer, with an average TM valence of 3.5+; furthermore, the 33.3% TM (all octahedral) in the 66.7%-Li (all tetrahedral) layer forms an ordered superlattice, imparting the system a cubic symmetry. The disordered rocksalt structure with the same chemical formula $Li(TM)O_2$ as the layered compound, on the other hand, destroys the planar Li–TM–Li–TM cation concentration wave

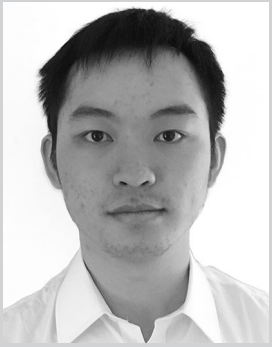

Yimeng Huang is a Ph.D. candidate in the Department of Materials Science and Engineering at the Massachusetts Institute of Technology. He received his B.S. in Eng. degree in Mechanical Engineering (UM-SJTU Joint Institute) from the Shanghai Jiaotong University and in Materials Science and Engineering from the University of Michigan in 2017. His current research interest is on advanced cathode materials for lithium-ion batteries.

Yanhao Dong is a postdoctoral researcher at the Massachusetts Institute of Technology. He obtained his BS degree in materials science in 2012 from the Tsinghua University, and his MS degree in materials science in 2014, his MS degree in applied mechanics in 2015, and his PhD degree in material science in 2017, all from the University of Pennsylvania. His current research interest is on the design, synthesis, and processing of ceramics and other materials, especially those for energy applications.

Ju Li is BEA Professor of Nuclear Science and Engineering and Professor of Materials Science and Engineering at MIT. His group performs computational and experimental research on mechanical properties of materials, and energy storage and conversion. He obtained a Ph.D. degree in nuclear engineering from MIT in 2000.

© 2020 WILEY-VCH Verlag GmbH & Co. KGaA, Weinheim

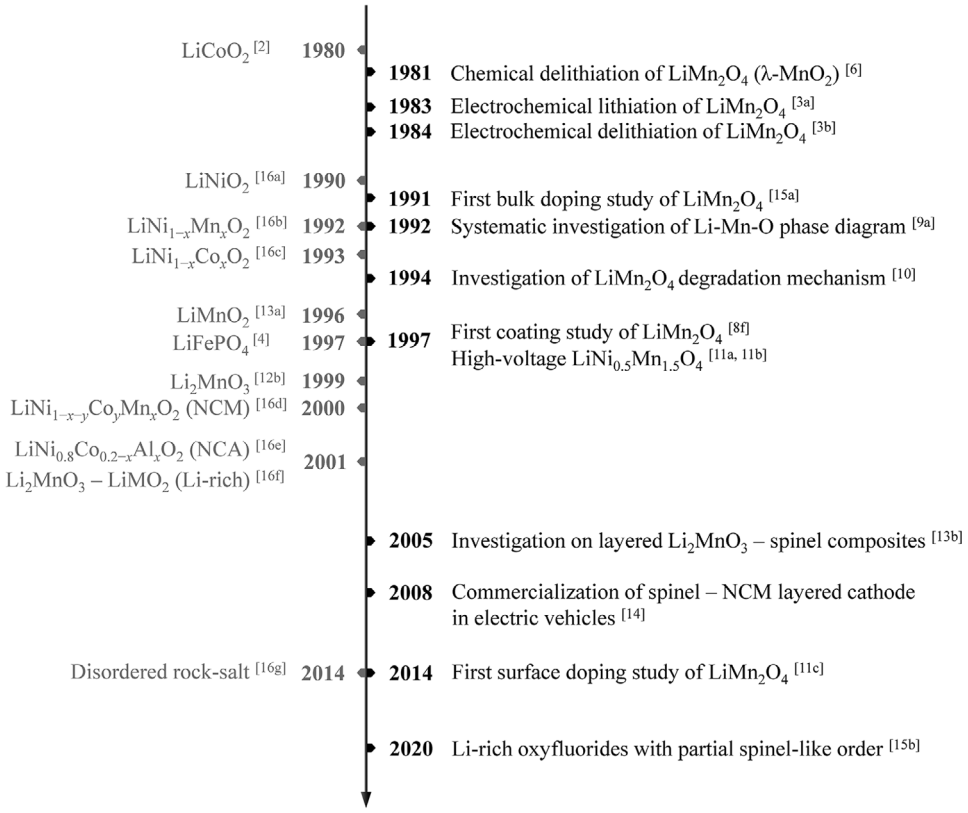

Figure 1. Development history of the spinel cathodes[3,6,8f,9a,10,11,13b,14,15] (right column) and the first studies of other major LIB cathodes (left column).[2,4,12b,13a,16]

altogether, and makes no distinction between layers, and there is only one cation sublattice (all octahedral) with equal occupation of Li/TM. This also recovers the cubic symmetry on average, as shown in the middle panel of Figure 3. Li-rich disordered rocksalt structure materials $Li_{1+x}(TM)_{1-x}O_2$ are under investigation as high-capacity cathodes, as long as there is sufficient "Li-richness" x (beyond the ideal reference structure) to ensure Li conduction percolation.[16g] After sufficient delithiation (oxidation) of the layered compound $Li(TM)O_2$, phase transformation from the layered structure in the top panel of Figure 3 to the spinel structure in the bottom panel requires out-of-plane migration of 1/4 of the Mn in the TM layer to the octahedral sites in the Li layer, while Li ions are displaced from octahedral to tetrahedral sites. The similarities in anion lattice and cation occupancy relate many Mn-based spinel and layered compounds, as shall be discussed later. Tetrahedral-to-octahedral displacement of Li can take place when lithiating spinel $Li(TM)_2O_4$ to create average composition $Li_{1+x}(TM)_2O_4$ ($0 < x < 1$), which is a two-phase reaction (spinel to ordered tetragonal rocksalt compound $Li_2(TM)_2O_4$) that provides a flat voltage plateau below 3 V versus Li^+/Li (**Figure 4**).[3a,27] The lithiation of $LiMn_2O_4$ is charge-compensated by Mn^{4+}/Mn^{3+}

Table 1. Comparison of common cathode materials in LIBs.

Material structure	Composition	Theoretical capacity [mAh g^{-1}]	Capacity at 0.1 C [mAh g^{-1}] (voltage range)	Operating voltage versus Li^+/Li [V]	Specific energy [Wh kg^{-1}]	Co/TM ratio	Cost	Refs.
Spinel	$LiMn_2O_4$	148	120 (3.0–4.3 V)	4.1	490	0	Low	[18]
	$LiNi_{0.5}Mn_{1.5}O_4$	147	125 (3.5–4.9 V)	4.7	590	0	Low	[19]
Layered	$LiCoO_2$	274	185 (3.0–4.45 V)	3.9	720	1	High	[20]
	$LiNi_{1/3}Co_{1/3}Mn_{1/3}O_2$	278	160 (2.8–4.3 V)	3.8	610	0.33	Medium	[21]
	$LiNi_{0.8}Co_{0.1}Mn_{0.1}O_2$	276	205 (2.8–4.3 V)	3.8	780	0.1	Medium	[21b,22]
	$LiNi_{0.8}Co_{0.15}Al_{0.05}O_2$	279	200 (2.8–4.3 V)	3.8	760	0.15	Medium	[23]
	$Li_{1.2}Ni_{0.13}Co_{0.13}Mn_{0.54}O_2$	377	240–270 (2.0–4.8 V)	3.6	860–970	0.16	Medium	[24]
Olivine	$LiFePO_4$	170	150 (2.5–4.2 V)	3.4	510	0	Low	[25]
	$LiMn_{0.8}Fe_{0.2}PO_4$	171	160 (2.5–4.2 V)	4.1	650	0	Low	[26]

© 2020 WILEY-VCH Verlag GmbH & Co. KGaA, Weinheim

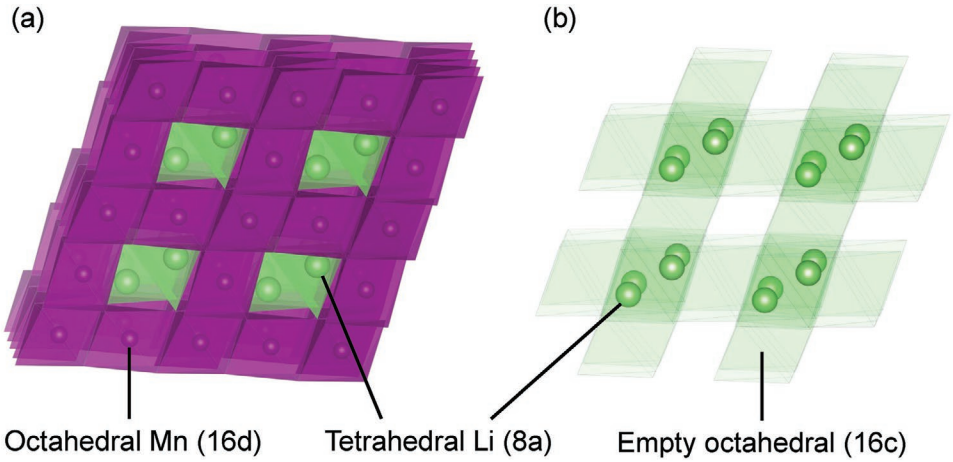

Figure 2. a) Crystal structure and b) Li^+ diffusion channel of $LiMn_2O_4$. Drawing based on work presented in ref. [28].

redox couple, where $Li_{1+x}Mn_2O_4$ has $(1+x)$ Mn^{3+} and $(1-x)$ Mn^{4+} on average with $x > 0$. Because octahedral Mn^{3+} ($t_{2g}{}^3e_g{}^1$) is a Jahn–Teller ion while Mn^{4+} ($t_{2g}{}^3e_g{}^0$) is not, excessive Mn^{3+} (over 1/2 of total Mn) in $Li_{1+x}Mn_2O_4$ initiates cooperative Jahn–Teller distortion in the lattice and disrupts the cubic symmetry (to tetragonal), which degrades the material upon electrochemical cycling. On the other hand, for delithiation of $LiMn_2O_4$, cubic symmetry can be maintained throughout the entire range of $0 < y < 1$ in $Li_{1-y}Mn_2O_4$, offering better structural stability during cycling. Furthermore, Li occupies a diamond-like array at 8a sites with two subsets of interpenetrating FCC Li patterns in $LiMn_2O_4$, where one ordered Li subset retains at $Li_{0.5}Mn_2O_4$ ($y = 0.5$) ideally. At this point, $LiMn_2O_4 \rightarrow Li_{0.5}Mn_2O_4$ would have given 74.1 mAh g^{-1} ($LiMn_2O_4$) charge capacity, with the rest 74.1 mAh g^{-1} ($LiMn_2O_4$) charge capacity from $Li_{0.5}Mn_2O_4 \rightarrow Li_0Mn_2O_4$ yet to come. Interestingly, Mn^{4+}/Mn^{3+} redox couple is very sensitive to Li^+ ordering, which leads to a small voltage step (≈0.15 V) between two voltage plateaus around 4 V versus Li^+/Li. This sensitivity also leads to a large voltage drop (>1 V, Figure 4) between $LiMn_2O_4$ and $Li_{1+x}Mn_2O_4$ as it involves tetrahedral-to-octahedral Li sublattice shift, which practically limits the cycling of Li to only ≈1 Li per two Mn from $[Mn_2]O_4$ to $Li[Mn_2]O_4$[27] in standard coarse-grained spinels.

$LiMn_2O_4$ has many derivatives that have similar chemistry and structures, indicated by many metastable compounds in Li–Mn–O phase diagrams constructed for either high-temperature synthesis or room-temperature chemical/electrochemical conversion.[9,10,30] One useful phase diagram near the $LiMn_2O_4$ composition is shown in **Figure 5**, originally constructed by Thackeray et al.[9b,10,30a] to investigate the effect of composition and Mn valence on the electrochemical properties of spinel and spinel-related materials. Spinel materials with the

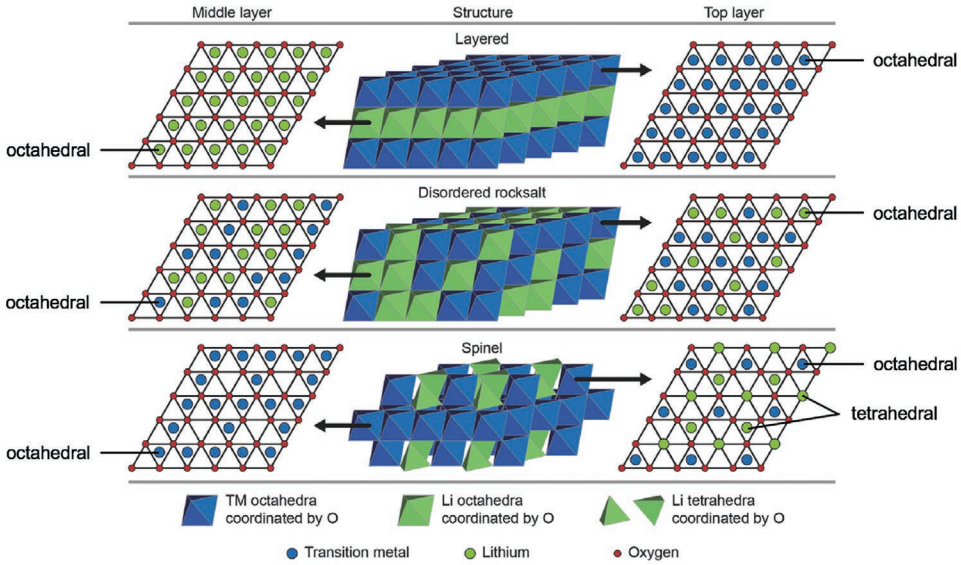

Figure 3. Schematic crystal structure and octahedral/tetrahedral site occupancy in layered (top panel), disordered rocksalt (middle panel) and spinel (bottom panel). Li occupancy is denoted by green circles/polyhedra. TM occupancy is denoted by blue circles/polyhedra. Different cation sizes and polyhedral distortions are omitted for simplicity. Reproduced with permission.[29] Copyright 2017, John Wiley & Sons, Inc.

© 2020 WILEY-VCH Verlag GmbH & Co. KGaA, Weinheim

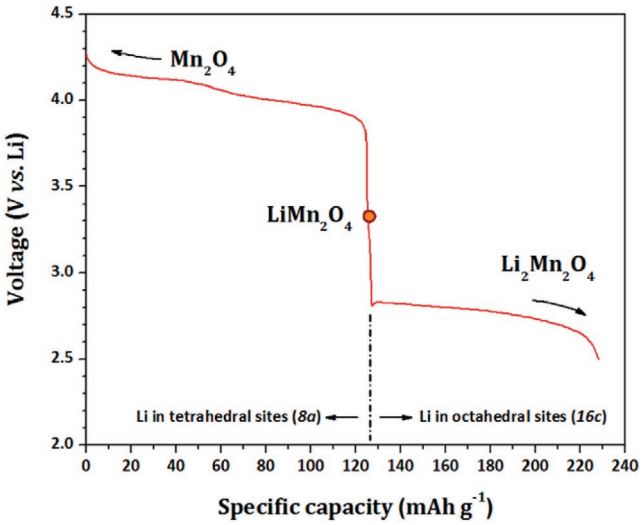

Figure 4. Voltage profile of $LiMn_2O_4$ during lithiation and delithiation. Reproduced with permission.[27] Copyright 2013, American Chemical Society.

greatest electrochemical interest lie on the "Spinel tie-line" connecting $LiMn_2O_4$ and $Li_4Mn_5O_{12}$ (equivalently $Li[Li_{1/3}Mn_{5/3}]O_4$), where Li substitutes up to 1/6 of the octahedral Mn with the chemical formula $Li_{1+x}Mn_{2-x}O_4$ (or $Li[Li_xMn_{2-x}]O_4$; $0 \leq x \leq 1/3$) while maintaining average cubic symmetry. Such "Li-rich spinel" $Li_{1+x}Mn_{2-x}O_4$ can be considered to be created by simultaneous lithiation and removal of Mn, which is not the same as pure lithiation, as is made clear by the different directions on the phase diagram in Figure 5. As mentioned above, pure lithiation of $LiMn_2O_4$ (along the dashed line from $LiMn_2O_4$ to the end product $Li_2Mn_2O_4 = LiMnO_2$, which can be rocksalt or layered) often triggers a spinel-to-ordered tetragonal rocksalt phase transformation due to reduced Mn valence (too much Mn^{3+} makes the system prone to Jahn–Teller distortion), while its delithiation (along the dashed line from $LiMn_2O_4$ to the end product λ-MnO_2) follows a solid-solution behavior. Similar trends apply to Li-rich spinel $Li_{1+x}Mn_{2-x}O_4$, where further lithiation enters the two-phase regime, and delithiation enters the cubic defect-spinel regime ($LiMn_2O_4$–$Li_4Mn_5O_{12}$–λ-MnO_2 triangle). Accompanied with Li substitution $Li_{1+x}Mn_{2-x}O_4$ (i.e., $Li[Li_xMn_{2-x}]O_4$) is the increase of average Mn valence to $(7-x)/(2-x)$, so that Mn^{4+}/Mn^{3+} redox couple can only provide $(1-3x)/(2-x)$ electrons per Mn and charge-compensate the removal of $(1-3x)$ Li ions, due to both increased average TM valence and decreased number of TM redox sites. Therefore, the Mn^{4+}/Mn^{3+} cation-redox capacity (proportional to the total length of the dashed line passing through the spinel composition in Figure 5) decreases dramatically with increasing Li-richness x. This means if a Li-rich spinel (an extreme case would be $x = 1/3$ or $Li_4Mn_5O_{12}$ where 100% of Mn valence is 4+) can still give significant charging capacity experimentally,[31] then part of this capacity must originate from oxygen redox, or HACR activities.[32] On the other hand, the increase of average Mn valence broadens the cubic spinel regime of $Li_{1+x}Mn_{2-x}O_4$ before transforming to tetragonal rocksalt phase, and also increases the average Mn valance to $(6-x)/(2-x)$ in fully lithiated product $Li_{2+x}Mn_{2-x}O_4$. The latter decreases c/a ratio in tetragonal rocksalt $Li_{2+x}Mn_{2-x}O_4$, e.g., from average valence of +3 and $c/a = 1.16$ in $Li_2Mn_2O_4$ to +3.4 and $c/a = 1.11$ in $Li_7Mn_5O_{12}$, which reduces the damaging Jahn–Teller effect.

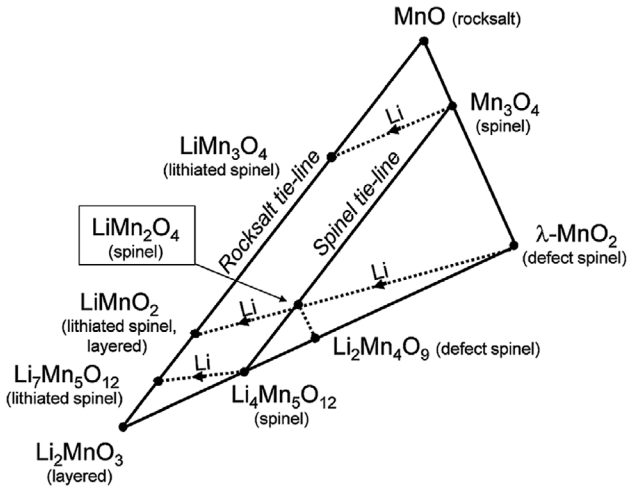

Figure 5. Li–Mn–O phase diagram near $LiMn_2O_4$ composition. Reproduced with permission.[30a] Copyright 2018, Royal Society of Chemistry.

Because of the versatile valence, stoichiometry, and polymorphism that Li–Mn–O-based compounds can adopt, the obtained phases strongly depend on synthesis methods and conditions.[30] For example, while $LiMn_2O_4$ is typically synthesized at higher temperatures >800 °C, $Li_4Mn_5O_{12}$ often forms at lower temperatures around 400 °C, and may result in impurity phases with other Li/Mn ratios; $LiMnO_2$ can have various crystal structures of rocksalt (tetragonal), layered (monoclinic), staggered configurations (orthorhombic), and their composites.[3a,13a,30a,33] The last and probably the most important derivative of $LiMn_2O_4$ is the high-voltage spinel $LiNi_{0.5}Mn_{1.5}O_4$, where Ni^{2+} substitution sets all Mn in +4 valence. It operates on Ni^{4+}/Ni^{2+} double redox at ≈4.7 V versus Li^+/Li, with a theoretical capacity of 147 mAh g^{-1} and a practical capacity of 125 mAh g^{-1}.[19] Because of the higher energy density and improved cycling stability, $LiNi_{0.5}Mn_{1.5}O_4$ has attracted continuous interest since its first reports in 1997.[11a,b]

3. Degradation Mechanisms of Spinel Cathodes

An ideal electrode for LIBs should be a partially closed system that only allows the removal and insertion of Li via ambipolar diffusion of Li^+ and electrons. It generally does not apply to real materials as side reactions take place at the interface between active electrode materials and organic liquid electrolytes, where there are often effluences of TMs and oxygen, especially at extreme potentials. The resultant solid products form a passivation layer between electrodes and electrolytes, known as solid–electrolyte interphases (SEIs) at the anode side and cathode–electrolyte interphases (CEIs) at the cathode side.[34] Gaseous products could evolve mainly in the form of O_2, CO_2, and others, as observed in differential electrochemical mass spectrometry measurements of charged cathodes and some anodes (e.g., $Li_4Ti_5O_{12}$).[35] These soluble products could enter the liquid electrolyte, e.g., the well-known problem of TM dissolution for

© 2020 WILEY-VCH Verlag GmbH & Co. KGaA, Weinheim

$LiMn_2O_4$ and other Mn-based cathodes.[36] This is an important issue, not only because it leads to the loss of active cathode materials, but also because the dissolved TM ions can migrate to the anode side under electric field and/or concentration gradient and deposit on the anode surface under a low potential (vs Li metal, and thus a reducing condition), as confirmed by various experimental techniques (e.g., energy-dispersive X-ray spectroscopy,[37] Rutherford backscattering spectroscopy,[8d] secondary ion mass spectrometry,[38] X-ray photoelectron spectroscopy (XPS),[8d,37b] and X-ray absorption near edge spectroscopy[39]). The deposited TMs are known to affect the SEI of graphite anodes that significantly degrades the battery,[11c,37a,40] and change the deposition/growth morphology of Li metal anodes[41] that are under intense development currently.[42] The problem of TM dissolution is arguably the Achilles' heel of $LiMn_2O_4$ and has been attracting continuous research interests over decades.

Before LIBs, Mn dissolution of $LiMn_2O_4$ was investigated by Hunter[6] in aqueous acidic solutions, which produced Li^+ and Mn^{2+} in the solution and λ-MnO_2 (with all Mn being +4 valence) at room temperature. Based on this observation, Hunter proposed a conversion reaction

$$2LiMn_2O_4 = Li_2O + 3MnO_2 + MnO \tag{1}$$

where Li_2O and MnO are soluble under acidic conditions, based on a disproportionation mechanism

$$2Mn^{3+} = Mn^{2+} + Mn^{4+} \tag{2}$$

at the surface. Outward ambipolar diffusion of Li^+ and electron polarons (**Figure 6**) then follows, until the bulk is turned into λ-MnO_2. This mechanism was followed and extended by Thackeray et al.[3b] in their first report of electrochemical delithiation of $LiMn_2O_4$, which proved that both Li^+ and electron polarons have sufficiently high lattice diffusivity at room temperature and modified the disproportionation mechanism by assigning different surface and bulk stabilities (denoted as subscripts) of $Mn^{2+/3+/4+}$

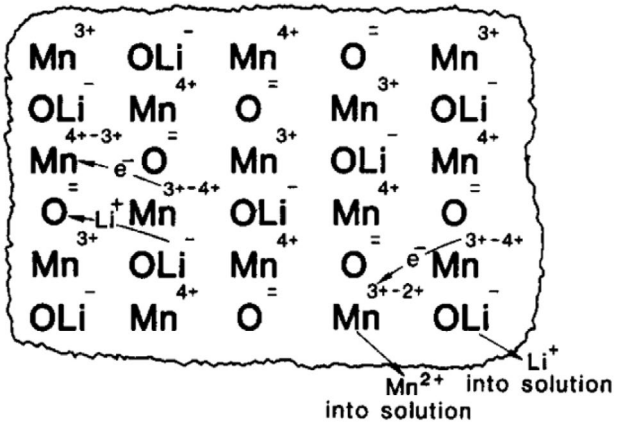

Figure 6. Schematic mechanism of the conversion of $LiMn_2O_4$ to λ-MnO_2 in aqueous acidic solutions. Reproduced with permission.[6] Copyright 1981, Elsevier Inc.

$$\left(Mn^{3+}\right)_{Surface} + \left(Mn^{3+}\right)_{Bulk} = \left(Mn^{2+}\right)_{Surface} + \left(Mn^{4+}\right)_{Bulk} \tag{3}$$

This mechanism is supported by the observations of Mn^{2+} in aqueous solutions[6] and organic electrolytes (by differential pulse polarography[43] and X-ray absorption near-edge structure spectra[44]), and is consistent with the observations that Mn dissolution becomes more severe with smaller particles and larger specific surface areas, higher acidity of the electrolyte, and higher temperatures.[3b,6,45] (There are two recent studies that reported Mn^{3+} as the main TM dissolution species of $LiMn_2O_4$ in battery electrolytes, while Mn^{2+} still being the main dissolution species of $LiNi_{0.5}Mn_{1.5}O_4$.[46] The investigation was followed by Hanf et al.[47] showing that Mn^{3+} is the main product of $LiNi_{0.5}Mn_{1.5}O_4$ in aqueous acidic solutions, while Mn^{2+} dominates in organic electrolytes.) Therefore, this disproportionation mechanism has been widely stated and discussed in the literature. However, it requires caution to treat Mn^{3+} disproportionation as the only cause of Mn dissolution. This is because if this mechanism dominates, Mn dissolution would be more pronounced as Mn valence decreases (which peaks at the lowest voltage at the end of discharge/lithiation) and less so as Mn valence becomes higher (which should cease at the highest voltage at the end of charge/delithiation); however, it has been shown by various experiments that Mn dissolution accelerates both in discharged states <3.1 V versus Li^+/Li and in charged states >4.1 V, and peaks at the highest voltage during charge.[43–45] The disproportionation argument again fails in $LiNi_{0.5}Mn_{1.5}O_4$, where all Mn are at +4 valence, yet Mn dissolution still takes place (albeit less than $LiMn_2O_4$) and accelerates at higher charge voltages.[40] The observed Mn dissolution under highly charged states indicates the surface instability of highly delithiated $LiMn_2O_4$ and $LiNi_{0.5}Mn_{1.5}O_4$, which could result in anion-redox-induced global oxygen mobility,[32] oxygen loss, TM reduction, and side reactions with the organic electrolytes. For example, with combined XPS, electron energy loss spectroscopy (EELS), scanning transmission electron microscopy (STEM), and density functional theory (DFT) calculations, Tang et al.[48] reported the reduction of surface Mn upon charging and oxidation of surface Mn upon discharging, which is contrary to what are expected in the bulk; Gao et al.[49] used atomic-level STEM to directly characterize and visualize oxygen loss, Mn reduction, and surface reconstruction upon charging; using epitaxial $LiMn_2O_4$ thin films, Hirayama et al.[50] showed that surface instability/reconstruction and Mn dissolution are surface dependent and more pronounced at (110) than at (111) surface. These observations have shed light on the fundamental mechanism of high-voltage instability of spinel cathodes, especially at the surface.[51] Conventionally, such surface instability was thought to be only applicable to redox couples that are pinned at the top of O-2p bands, e.g., Co^{4+}/Co^{3+} redox couple in $LiCoO_2$. But, as is clear in the example of $LiMn_2O_4$, the anion-redox-led structural instability could be stronger at the surface than in the bulk, and surface oxygen loss accompanied by TM reduction and surface reconstruction should be general in most of the high-voltage cathode materials. The as-reduced TMs can lead to surface phase transformation, and in the case of $LiMn_2O_4$ and other Mn-based cathodes, TM dissolution in the form of Mn^{2+}.

© 2020 WILEY-VCH Verlag GmbH & Co. KGaA, Weinheim

Beyond TM dissolution that causes loss of active cathode materials, there are also surface phase transformations that increase the impedance of cathodes.[52] Both factors contribute to capacity decay and quantitatively, the loss of active materials was found to be only responsible for 20–30% of the overall capacity decay.[43] The impedance growth is attributed to surface phase transformation with poor Li^+ diffusivity, which happens at both ends of charge and discharge, especially under fast charging/discharging, nonequilibrium conditions, and prolonged cycling. At the end of discharge, the damaging Jahn–Teller distortion[53] could initiate at the surface and induce cubic-to-tetragonal phase transformation, where ordered tetragonal rocksalt $Li_2Mn_2O_4$ phase was observed at the surface of $LiMn_2O_4$ cycled between 3.3 and 4.2 V versus Li^+/Li.[54] At the end of charge, on the other hand, oxygen escape leads to the formation of Mn_3O_4 (with average Mn valence of +8/3, less than +3) phase at the surface, which produces soluble Mn^{2+}.[48] Such electrochemically induced phase transformations were recently investigated by Liu et al.[55] via advance characterizations of combining in situ synchrotron high-resolution X-ray diffraction (XRD), X-ray absorption spectroscopy, X-ray fluorescence, and STEM. The results (**Figure 7**) clearly reveal the formation of Mn_3O_4 at upper charge voltage of 4.3 V versus Li^+/Li and the formation of $Li_2Mn_2O_4$ at lower discharge voltage of 3.4 V versus Li^+/Li. The phase transformations are partially irreversible and lead to particle cracking upon cycling, which further causes detrimental increase in reactive surface area. Similar observations of Mn_3O_4-like structures ("bad spinel") have also been reported by Lin et al.[56] on the surface (about 2 nm thick) of $LiNi_{0.5}Mn_{1.5}O_4$ during the first charge up to 4.9 V versus Li^+/Li, whereas a rocksalt-like structure was observed in the subsurface region. Interestingly, it was shown by Amos et al.[57] by aberration-corrected STEM that the surface of uncycled $LiMn_2O_4$ can automatically reconstruct into a thin surface layer of Mn_3O_4 ("bad spinel," which is also electrolyte soluble) and a subsurface layer of $Li_{1+x}Mn_2O_4$ near the surface of a bulk $LiMn_2O_4$ particle (**Figure 8**), which indicates surface oxygen deficiency and a subsequent disproportionation reaction. The blockage of the 3D Li^+ diffusion channels in Mn_3O_4-like and rocksalt-like structures is likely to be the reason why the transformed phases dramatically increase cell impedance.

The observed TM dissolution, oxygen escape, surface reconstruction, and surface phase transformations point to the

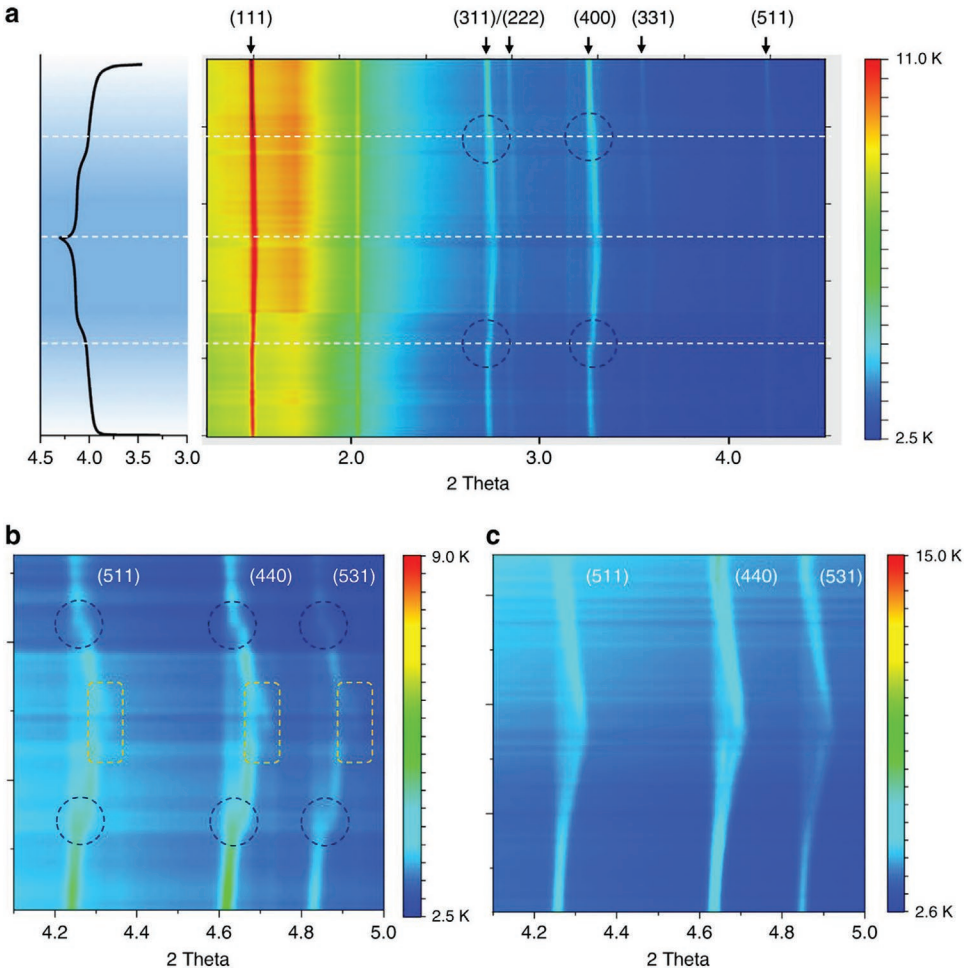

Figure 7. a) In situ synchrotron high-resolution X-ray diffraction of $LiMn_2O_4$ for the first charge and discharge between 3.4 and 4.3 V versus Li^+/Li. b) Enlarged view of (a). c) Enlarged view of similar measurements performed on $Li_{1.1}Mn_{1.9}O_4$ for the first charge and discharge between 3.4 and 4.3 V versus Li^+/Li. Reproduced with permission.[55] Copyright 2019, Springer Nature.

© 2020 WILEY-VCH Verlag GmbH & Co. KGaA, Weinheim

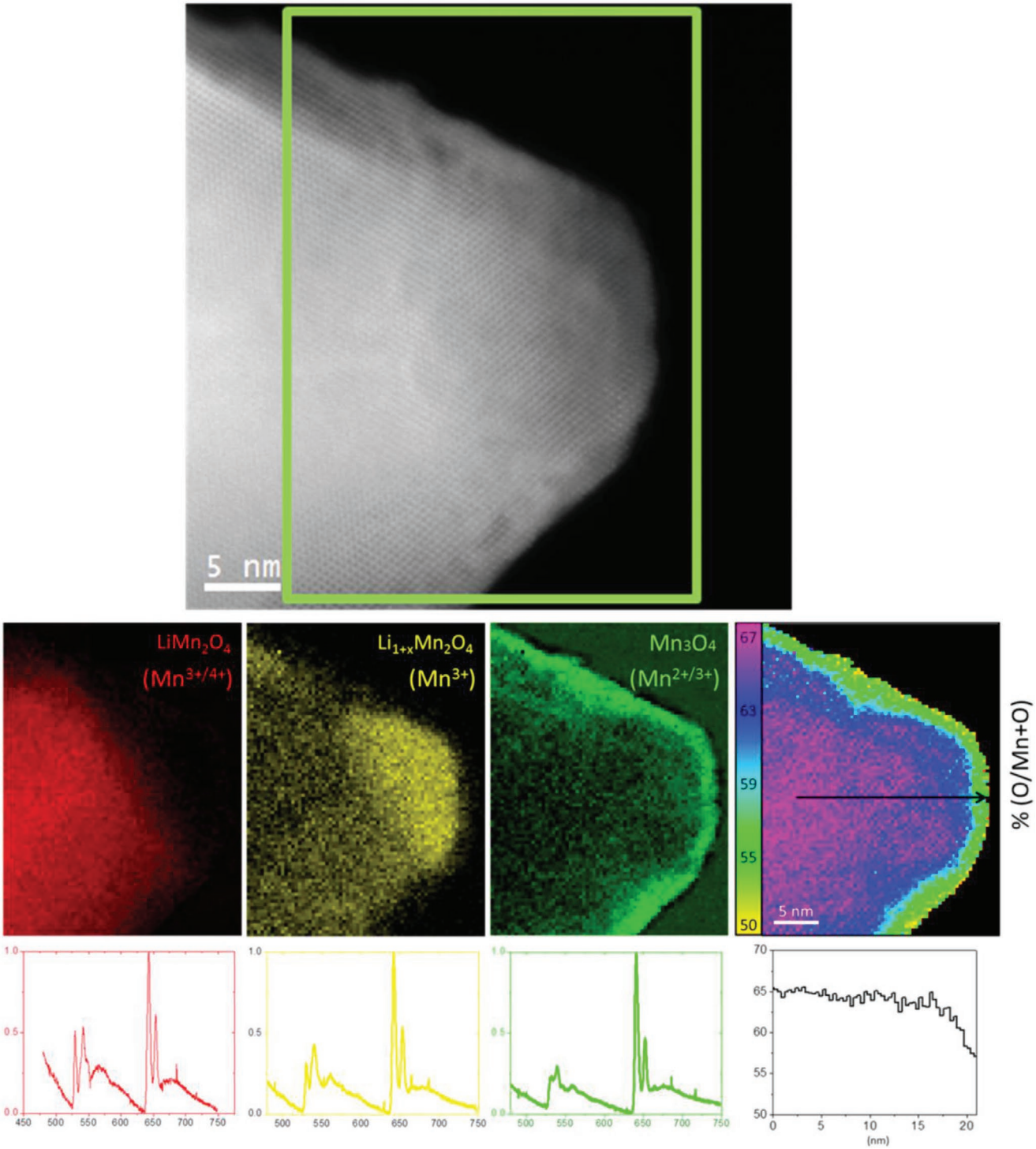

Figure 8. High-angle annular dark-field imaging (HAADF) STEM image of a $LiMn_2O_4$ particle, with green rectangle showing the inspected area (top panel). Colored maps (red, yellow, and green) and the corresponding EELS spectra (in the same color) representing the location of different Mn valence states, and a map showing atomic ratio of O/(Mn+O) calculated from the O K edge and Mn $L_{2,3}$ edge (middle and bottom panels). Reproduced with permission.[57] Copyright 2016, American Chemical Society.

critical role of the interactions between the cathode surface and the electrolyte under dynamic conditions, which are still not well understood at the present stage. On one hand, surface structure and chemistry of the spinel cathodes need to be better characterized and studied, as a function of crystal orientations, terminating species, segregating cations, and electrochemical potentials. Special attention should be paid to the surface phase stability and diffusion kinetics of Li^+ and TM species

© 2020 WILEY-VCH Verlag GmbH & Co. KGaA, Weinheim

in pristine and transformed surface structures. In addition to various advanced experimental tools, first-principles calculations should help to construct a database and offer mechanistic insights. For example, stability and phase diagram of $LiMn_2O_4$ (001) and (111) surfaces have been evaluated and constructed by Kim et al.[58] using DFT calculations with different terminations and at various chemical potentials of lithium, which suggest that (111) surfaces with Li-rich surface layers are more resistant to Mn dissolution than (001) surfaces. Ti and Ta surface doping have been shown by DFT calculations to promote the formation of rocksalt phase, lower Ni valence under fully charged state, and stabilize the oxygen framework of $LiNi_{0.5}Mn_{1.5}O_4$, which suggest suppressed side reactions and oxygen evolution during electrochemical cycling.[59] Such simulations would offer valuable insights to the experimental design of particle morphology, surface composition, and others. On the other hand, it is more challenging to understand the complicated interactions at the solid–liquid interface during electrochemical cycling, especially the formation and dynamic evolution of CEIs, decomposition and oxidation of organic electrolytes, and surface diffusion, solvation, and dissolution of Mn and other TM species. It again requires synergetic efforts with various ex situ and in situ characterization tools (e.g., time-of-flight secondary-ion mass spectroscopy,[60] ultraviolet–visible spectroscopy[61]) and advanced simulation techniques (e.g., ab initio molecular dynamics simulations[61,62]) to capture and understand the underlying thermodynamics and dynamics, which could help to design stable artificial CEIs, novel electrolytes, and additives to fully solve the TM dissolution problem. Such mechanistic understandings hold the key for the future development of spinel cathodes.

4. Future Development of Spinel Cathodes

Because of the above issues of TM dissolution and surface phase transformations, spinel cathodes suffer from severe degradation especially during high-temperature cycling (e.g., at 50 °C), and there have been tremendous efforts to improve cycling and rate performance. First of all, bulk doping is the most practiced method. For $LiMn_2O_4$, considering the disproportionation mechanism of Mn^{3+}, it is beneficial to increase the average Mn valence, which is possible by lower-valence (less than or equal to +3) cation doping. Many dopants (including Li^+, Mg^{2+}, Zn^{2+}, Ni^{2+}, Co^{2+}, Cr^{2+}, Cu^{2+}, Al^{3+}, Fe^{3+}, and Sc^{3+})[10,55,63] have been reported to improve cycling properties of $LiMn_2O_4$, among which doping with slightly excess Li is one of the simplest and most efficient method. Note that Li richness improves cycling at the expense of the available Mn^{4+}/Mn^{3+} cation-redox capacity, and thus lowering the cation-redox capacity. The anion-redox capacity would need to be activated at higher charging voltages. Such a trade-off needs to be considered in stabilizing $LiMn_2O_4$. Meanwhile, successful dual- and multication doping strategies have been reported, which opens a larger compositional space for optimizations that could be assisted by machine learning.[64] For example, Xiong et al.[63f] recently reported that $Cu^{2+}/Al^{3+}/Ti^{4+}$ multication doping has a synergetic effect to improve the cycling stability of $LiMn_2O_4$. Meanwhile, higher-valence (above +3) cation doping (e.g., Ti^{4+})[63c,d] and anion substitution with F^-[63e,65] were also reported to improve the cycling of $LiMn_2O_4$. This seems counterintuitive at first glance as they would lower Mn valence and hence should not be beneficial. Nevertheless, their effectiveness suggests the complicated role of doping atoms most likely in the surface structure and chemistry, which is worthwhile for future studies especially via advanced experimental and simulation techniques. On the other hand, doping with electrochemically active elements led to the development of $LiNi_{0.5}Mn_{1.5}O_4$, where Ni^{2+} sets all Mn at +4 valence that makes the structure stable. Albeit with similar capacity, $LiNi_{0.5}Mn_{1.5}O_4$ has higher energy density (because $Ni^{4+/2+}$ operates at a higher redox potential at ≈4.7 V vs Li^+/Li without sacrificing capacity[66]) and better cathode stability than $LiMn_2O_4$. However, the large-scale application of $LiNi_{0.5}Mn_{1.5}O_4$ is hindered by the obstacle to commercialize a stable 5 V electrolyte. Nevertheless, the intrinsic high-voltage stability of $LiNi_{0.5}Mn_{1.5}O_4$ also leads to various doping studies, including Mg^{2+}, Fe^{3+}, Co^{3+}, Cr^{3+}, Al^{3+}, and Ru^{4+}, to further increase cycling performance.[67] A recent work by Liang et al.[67a] explored site-selective Mg doping in both tetrahedral (8a) and octahedral (16c) sites and demonstrated excellent cycling stability with 86% capacity retention after 1500 cycles at 1 C and 87% capacity retention after 2200 cycles at 10 C. Furthermore, engineering the oxygen stoichiometry was explored in spinel cathodes.[8c,d] Considering the complicated Li–Mn–O phase diagram and the sensitivity on synthesis condition and methods, precise control of the oxygen stoichiometry and defects may be challenging, but may also provide new opportunities in novel phases and/or composites with good properties.

Second, in addition to bulk doping, it is also important to tailor the dopant distributions. It was well recognized that in $LiNi_{0.5}Mn_{1.5}O_4$, different levels of Ni/Mn cation ordering (controllable by synthesis conditions) give rise to variations in capacity and cycling stability.[68] Such cation ordering in the bulk lattice originates from strong cation–cation interactions and would be smeared out with larger contributions of configuration entropy. Therefore, it should be general in many other heavily doped spinel cathodes, especially for the dopants with very different size and charge, strong magnetic interactions, and when using low-temperature synthesis methods. This ordering phenomenon is worthwhile to be studied in the future, especially the influence of chemical short-range order (SRO) on electrochemical kinetics. Apart from dopant distributions in the bulk, surface doping is now recognized as an efficient method to stabilize spinel cathodes, as the capacity is minimally affected by the trace amounts of electrochemically inactive dopants.[69] This strategy was first reported by Lu et al.,[69a] where a thin layer of TiO_2 was coated on the surface of $LiMn_2O_4$ via atomic layer deposition or sol–gel method followed by heat treatment. The obtained Ti-surface-doped $LiMn_2O_4$ showed improved cycling with suppressed Mn dissolution and less impedance growth. A recent progress has been made by Piao et al.,[69b] where site-selective (occupying empty 16c octahedral sites) Al surface doping can dramatically improve cycling (97.6% capacity retention after 150 cycles at 0.1 C) and rate performance of $LiNi_{0.5}Mn_{1.5}O_4$. The surface doping approach could be obtained by two ways: from the kinetic perspective, one can uniformly coat the cathode particles by wet-chemistry or vapor-deposition methods, followed by a low-temperature and/or short-time annealing to suppress long-range cation diffusion; from the thermodynamic perspective, one can

© 2020 WILEY-VCH Verlag GmbH & Co. KGaA, Weinheim

use dopant elements that tend to segregate at the surface. We believe this promising approach would lead to fruitful results in the future development of spinel cathodes.

Third, surface coating is another commonly practiced method to improve cycling performance, with a wide range of coating materials, including oxides (e.g., $Li_2O:B_2O_3$, Al_2O_3, ZrO_2, ZnO, SiO_2, Li_2ZrO_3, and $LiNi_{1-x}Co_xO_2$),[8f,70] fluorides (e.g., AlF_3),[71] phosphates[72] (e.g., $Li_3V_2(PO_4)_3$[73]), and polymers.[74] With recent development in solid electrolytes for LIBs, coating spinel cathodes with fast Li^+ conductors such as $Li_{6.4}La_3Al_{0.2}Zr_2O_{12}$ has also attracted attention.[75] Typically, the coating layer can physically separate the contact between active cathode materials and organic electrolytes and suppress side reactions such as Mn dissolution. In other words, it should be less reactive to the electrolyte and catalytically active than the bare spinel cathodes under dynamic conditions. Meanwhile, it should have a minimal effect on the impedance, with the ideal one having a good lattice match with spinel cathodes and being a good Li^+ and electronic conductor. Moreover, it is important to achieve uniform thin coating with good wetting properties, which remains conformal and all-covering not only in the pristine state but also during electrochemical cycling. Therefore, despite of much progress that has been achieved, more investigations on new materials and scalable cost-effective synthesis methods are required to optimize the coating of spinel cathodes.

Fourth, the morphology of spinel cathodes can be tuned to improve cycling. While nanomaterials[76] are attractive due to short diffusion length, good stress relief and damage tolerance, and other intriguing properties, coarse-grained $LiMn_2O_4$ with smaller specific surface area and hence less side reactions is more desirable in terms of cycling stability. The particle size effect on Mn dissolution was observed in Hunter's experiments and later discussed by Thackeray et al.[3b,6] Previous experimental and simulation results also suggest different stability and Mn dissolution rates at surfaces with different surface inclinations, so it could be beneficial to control the shape and crystal orientation of the particles. This could be achieved by molten salt method and tuned by different liquid–solid interfacial interactions during high-temperature synthesis. Since the low-cost solid-state synthesis is the preferred route for large-scale production, the interplay among particle size, dispersion, crystallinity, and electrochemical properties should be also tailored by adjusting the heat-treatment schedule and different precursors/raw materials. Such a knowledge of know-how is a nontrivial issue that deserves detailed studies and optimizations, probably with the aid of the recently developed machine learning and high throughput strategies. Meanwhile, different synthesis methods and heat-treatment processes would influence defects (e.g., oxygen vacancy) and cation ordering, which should be considered to separate the processing and chemical effects on the electrochemical performances.

Fifth, modifications of the organic liquid electrolytes could be beneficial. Previous studies in $LiMn_2O_4$ have shown that additives such as $(CH_3)_3SiNHSi(CH_3)_3$, lithium bis(oxalato) borate (LiBOB), $CaCO_3$, and pyridine could help improve cycling, either due to the formation of a more stable surface phase or through scavenging the damaging HF in the organic electrolytes.[77] Meanwhile, advanced liquid electrolytes for LIBs and other aqueous/nonaqueous batteries are under rapid development in recent years.[78] For example, Chen et al.[79] reported stable cycling of $LiMn_2O_4$ cathodes (paired with $Li_4Ti_5O_{12}$ anodes) in 2.5 V aqueous LIBs using superconcentrated aqueous electrolytes. For $LiNi_{0.5}Mn_{1.5}O_4$, Suo et al.[80] recently reported a class of full-fluoride electrolyte that enables highly stable 5 V-class lithium metal batteries, demonstrating >130 cycles at 0.36 C with slightly excess (1.4×) lithium as the anode and a high-loading $LiNi_{0.5}Mn_{1.5}O_4$ cathode (14.7 mg cm^{-2}, 1.83 mAh cm^{-2}). Note that the development of advanced electrolytes and additives for $LiMn_2O_4$ is relatively less explored compared to the extensively practiced doping and coating strategies, and commercialization of $LiNi_{0.5}Mn_{1.5}O_4$ is also hindered by the lack of high-performance 5 V electrolyte. Therefore, there is plenty of room for the development of novel liquid electrolytes, which may provide a good solution for spinel cathodes, including the challenging problem of high-temperature cycling.[81]

Finally, the application of spinel cathodes in all-solid-state batteries could be a by-pass solution to the TM dissolution problem in liquid electrolytes. Some solid electrolytes are kinetically stable at 5 V versus Li^+/Li, which could enable the use of $LiNi_{0.5}Mn_{1.5}O_4$. Spinel cathodes with cubic symmetry, 3D diffusion channel, and isotropic chemical expansion during electrochemical cycling also fit well with solid electrolytes. Preliminary results in the literature have reported successful usage of $LiMn_2O_4$ and $LiNi_{0.5}Mn_{1.5}O_4$ in bulk-type all-solid-state batteries with solid polymer electrolytes (e.g., polyoxyethylene-based[82] and polycarbonate-based polymer electrolytes[83]), sulfide-based solid electrolytes (e.g., $Li_2S–P_2S_5$[84] and $Li_{10}GeP_2S_{12}$[85]), and oxide-based solid electrolytes (e.g., $Li_{1.4}Al_{0.4}Ti_{1.6}(PO_4)_3$[86]), as well as thin-film-type all-solid-state batteries (with lithium phosphorus oxynitride (LiPON)[87] and $Li_{0.17}La_{0.61}TiO_3$[88] solid electrolytes). Note that there are many more reports on full cells using solid polymer electrolytes than using sulfide-based solid electrolytes, and there are few reports on full cells using oxide-based solid electrolytes, which suggest challenges in processing all-solid-state batteries with inorganic electrolytes, especially oxides. It also implies that even though oxide-based electrolytes such as garnet-structure $Li_7La_3Zr_2O_{12}$ has higher modulus (which is argued to be able to suppress lithium dendrite penetration) and larger voltage stability window, how to process them remains a great challenge. The high-temperature sintering process also raises the interdiffusion problem and potential formation of impurity phases, which have been reported in the literature.[86a,89] Another important challenge is the interfacial stability between spinel cathodes and solid electrolytes during electrochemical cycling, including wetting and contact, chemical compatibility, and electrochemical stability. Coating of spinel cathodes may still be necessary to address the interfacial problem. For example, amorphous $Li_4Ti_5O_{12}$ and Li_3PO_4 thin-film coatings were reported to improve the electrochemical performance of $LiMn_2O_4$ and $LiNi_{0.5}Mn_{1.5}O_4$ in all-solid-state batteries, respectively.[84b,c] For high-rate applications that require high power density and/or fast charging, even though spinel cathodes have good diffusion kinetics, most solid electrolytes have limited critical current density, beyond which fast electrolyte degradation and shorting would occur. Therefore, more development in the processing technique, interfacial stability, coatings, and solid electrolytes are required to achieve

© 2020 WILEY-VCH Verlag GmbH & Co. KGaA, Weinheim

practical applications of spinel cathodes in advanced all-solid-state batteries.

5. Spinel Structure as Degradation Product and Structural Stabilizer for Layered Cathodes

While the above content focuses on spinel cathodes, particularly on $LiMn_2O_4$ and $LiNi_{0.5}Mn_{1.5}O_4$, below we will discuss how stability and high rate performance of the spinel structure could help to design better LIB cathodes. This section focuses on the stability of the spinel structure that justifies its presence in various degraded layered cathodes and how it is integrated into layered cathodes to improve performance.

First of all, in nature, spinel represents a large family of minerals with a general formula of AB_2X_4, including spinel $MgAl_2O_4$ (which this mineral family and the structure are named after), gahnite $ZnAl_2O_4$, magnetite Fe_3O_4 (i.e., $Fe^{2+}(Fe^{3+})_2O_4$), cuprospinel $CuFe_2O_4$, chromite $FeCr_2O_4$, and many others.[90] The presence of such abundant minerals with versatile chemistry illustrates the phase stability of the spinel structure. This phase stability applies to battery-related transition metal oxides as well. For example, according to the phase diagram calculated by Materials Project,[91] spinel is the thermodynamically stable structure for both $LiNi_2O_4$ and $LiCo_2O_4$ compositions, which has been proved by in situ heating experiments.[92] Second, electrochemically, the stability of spinel is implied by the high voltages of TM redox couples in the spinel structure. For example, in spinel cathodes, Ni^{3+}/Ni^{2+} has a redox potential of about 4.6 V versus Li^+/Li, Ni^{4+}/Ni^{3+} has a redox potential of about 4.8 V versus Li^+/Li, Mn^{4+}/Mn^{3+} has a redox potential of about 4.0 V versus Li^+/Li, and Mn^{5+}/Mn^{4+} has a redox potential well above 5.0 V versus Li^+/Li.[93] These redox voltages are generally much higher than their respective values in layered cathodes, if we consider the average discharge voltage of about 3.8 V versus Li^+/Li for Ni-rich cathodes (that mainly operate on Ni^{4+}/Ni^{3+}) as a reference.[94] (Note that the redox potentials are even higher in olivine-structure phosphates, with Ni^{3+}/Ni^{2+} of about 5 V, Ni^{4+}/Ni^{3+} of about 5.3 V, and Mn^{4+}/Mn^{3+} of about 4.8 V vs Li^+/Li, which is also a structure with high stability.[95]) Such high redox voltages could be understood by the site energy of Li^+. In spinel cathodes, Li^+ reside in tetrahedral sites that are corner-shared with neighboring TM—O octahedra, while in layered cathodes, Li^+ reside in octahedral sites that are edge-shared with neighboring TM—O octahedra. With longer Li–TM distances, Li^+ in spinel cathodes experience less Coulombic repulsion from neighboring cations and are thus more energetically stable, compared to the case in layered cathodes. This raises the equilibrium voltage of TM redox because adding/removing electrons in LIB electrodes must also involve simultaneous insertion/removal of Li^+ to compensate charge. On the other hand, the high redox voltages should not come from contribution by electronic energy. This is because strong hybridization between TM 3d orbitals and oxygen 2p orbitals increases the energy of TM—O antibonding states (thus lowering TM cation-redox voltages) and lowers the energy of TM—O bonding states (thus increasing O anion-redox voltages). Atomistically, the hybridization could be stronger than the layered case considering the higher average TM valence of +3.5 in spinel cathodes than in layered cathodes, which results in stronger Coulombic attraction between TM and oxygen ions and creates shorter TM—O bonds. This strong hybridization is further supported by the inaccessible oxygen redox with a band edge at about 5.0 V versus Li^+/Li,[96] compared with the Li–O–Li-configuration-enabled oxygen redox at about 4.5 V versus Li^+/Li in Li-rich layered cathodes.[97] As a result, anion redox is typically not observed in $LiMn_2O_4$ nor $LiNi_{0.5}Mn_{1.5}O_4$, even up to 5.0 V versus Li^+/Li for the latter.[15b]

However, in Li-rich spinel such as $Li_4Mn_5O_{12}$ where Li substitute some of the Mn, TM—O hybridization becomes weaker, upshifting the O-orbital energy level and rendering anion redox accessible at a lower voltage. Liu et al.[31] recently reported HACR[32] activities in a Li-rich spinel with nominal composition close to $Li_4Mn_5O_{12}$, where oxygen anion-redox (*m*,*a*-contribution) and TM cation-redox (*p*,*c*-contribution) reactions could give a theoretical capacity of 243.9 mAh g^{-1} (illustrated in **Figure 9**). Some oxygen loss in the initial formation cycles could reduce the average valence of Mn, and cause increasing proportion of cation redox in later cycles, but reversible oxygen anion redox are likely still present. Due to the low-temperature (400 °C) solid-state synthesis, the primary particle sizes are small, and smaller cathode particles seem to tolerate Mn^{3+} Jahn–Teller distortion better.

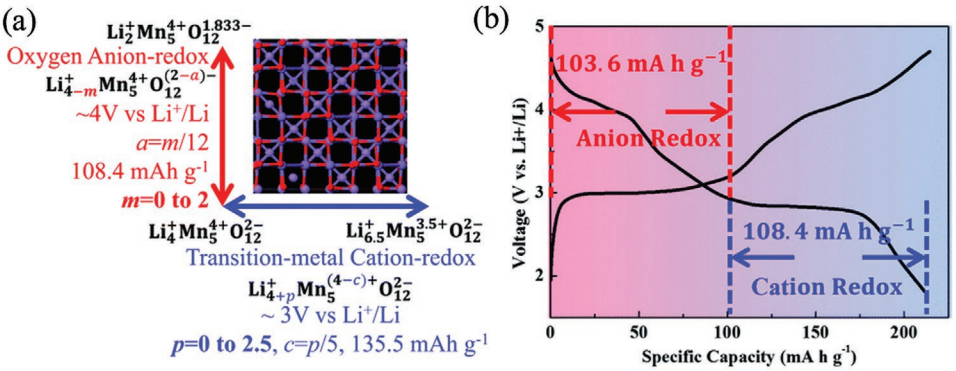

Figure 9. a) Hybrid oxygen anion-redox and TM cation-redox reaction coordinate as: $Li_2^+Mn_5^{4+}O_{12}^{1.833-} \leftrightarrow Li_4^+Mn_5^{4+}O_{12}^{2-} \leftrightarrow Li_{6.5}^+Mn_5^{3.5+}O_{12}^{2-}$. The inset shows spinel $Li(Mn_{5/3}Li_{1/3})O_4$ with long-range order of the 1/6 Li_{Mn} substitutions. b) Voltage profile of the $Li_4Mn_5O_{12}$-like half cells at the 20th cycle at a current density of 100 mA g^{-1} cycled between 1.8 and 4.7 V versus Li^+/Li at room temperature. Reproduced with permission.[31] Copyright 2019, Royal Society of Chemistry.

© 2020 WILEY-VCH Verlag GmbH & Co. KGaA, Weinheim

Finally, spinel cathodes are known for high thermal runaway temperature and good safety, which suggest good thermal stability. The aforementioned phase, structural, electrochemical, and thermal stability of the "good spinel" $Li(TM)_2O_4$ structures as well as "bad spinel" structures like $(TM)_3O_4$ where all conduction channels are blocked, correlate with their frequent appearances on the surface of various layered cathodes, especially under high voltages, high temperatures, and prolonged cycling. For example, the following observations were reported in $LiCoO_2$: using transmission electron microscopy (TEM) and electron diffraction, Wang et al.[98] observed cation occupancy at 8a tetrahedral sites and partial phase transformation to spinel-type ordering at the surface of $LiCoO_2$ cycled between 2.5 and 4.35 V versus Li^+/Li; Yazami et al.[99] observed the formation of cubic spinel phase under TEM in $LiCoO_2$ after aging at 4.7 V versus Li^+/Li for 10 h as well as irreversible loss in capacity and rate capabilities; using EELS, Kikkawa et al.[100] observed Co_3O_4-like phase and Li-inserted Co_3O_4 at the surface of $LiCoO_2$ charged to 40%, 60%, and 100% capacity; using HAADF-STEM and EELS, Tan et al.[101] observed Co_3O_4-like phase at the surface of epitaxial $LiCoO_2$ electrode films after charged to 4.2 V versus Li^+/Li; using HAADF-STEM, Yano et al.[102] observed spinel-like phase at the surface of $LiCoO_2$ cycled at 2.5–4.7 V versus Li^+/Li; using high-resolution TEM (HRTEM), Seong et al.[103] reported the formation of disordered spinel $Li_2Co_2O_4$ phase and spinel Co_3O_4 nanoparticles at the surface of $LiCoO_2$ cycled at 3.0–4.6/4.8 V versus Li^+/Li; and Yoon et al.[35b] observed spinel-like phase (**Figure 10**) at the surface of $LiCoO_2$ cycled at 3.0–4.45 V versus Li^+/Li, while 5% Ni doping is effective in modifying the production of the surface phase transformation to a cation-mixed phase. Similar observations were also made in NCM/NCA with various Ni/Co/Mn/Al ratios. For example, Nam et al.[104] used in situ synchrotron X-ray diffraction/absorption technique and TEM to study the structural evolution of overcharged $LiNi_{1/3}Co_{1/3}Mn_{1/3}O_2$ and $LiNi_{0.8}Co_{0.15}Al_{0.05}O_2$, and showed by XRD (**Figure 11**) that $Li_{0.33}Ni_{1/3}Co_{1/3}Mn_{1/3}O_2$ transformed to a spinel phase at 337 °C, while $Li_{0.33}Ni_{0.8}Co_{0.15}Al_{0.05}O_2$ transformed to mixed phases of spinel and rocksalt at 256 °C before turning into pure rocksalt at 471 °C. Jung et al.[105] observed minor rocksalt phase and dominating spinel phase at the surface of $LiNi_{0.5}Co_{0.2}Mn_{0.3}O_2$ cycled at 3.0–4.5 V versus Li^+/Li, and spinel phase enclosed by rocksalt phase at the surface of $LiNi_{0.5}Co_{0.2}Mn_{0.3}O_2$ cycled at 3.0–4.8 V versus Li^+/Li, while $LiNi_{0.5}Co_{0.2}Mn_{0.3}O_2$ cycled at 3.0–4.3 V versus Li^+/Li shows little phase transformation. Lin et al.[106] used atomic resolution annular dark-field STEM to investigate the surface reconstruction of $LiNi_{0.4}Mn_{0.4}Co_{0.18}Ti_{0.02}O_2$ and found a thin layer of spinel structure bridging the untransformed layered structure (with Ni^{2+}, Mn^{4+}, and Co^{3+}) and the transformed rocksalt structure (with Ni^{2+}, Mn^{2+}, and Co^{2+}). Using HAADF-STEM and electron diffraction, Kim et al.[107] observed the formation of spinel structure around microcracks inside the primary particles of $LiNi_{0.6}Co_{0.2}Mn_{0.2}O_2$ cycled at 3.0–4.45 V versus Li^+/Li at 60 °C.

Transformation to spinel is more pronounced in layered Li-rich cathodes that utilize both cation (TM) and anion (O) redox. For example, with combined XRD, high-resolution TEM, and Raman spectroscopy, Hong et al.[108] confirmed the transformation to spinel-like domains in the layered framework of $Li_{1.2}Ni_{0.2}Mn_{0.6}O_2$ cycled at 2.0–4.8 V versus Li^+/Li. Similarly, Ito et al.[109] observed by atomic resolution HAADF-STEM and selected-area electron diffraction (SAED) the formation of the spinel structure in $Li_{1.2}Ni_{0.17}Co_{0.07}Mn_{0.56}O_2$ at 4.5 V plateau during the first charge to 4.8 V versus Li^+/Li, Xu et al.[110] observed the formation of a defect-spinel phase

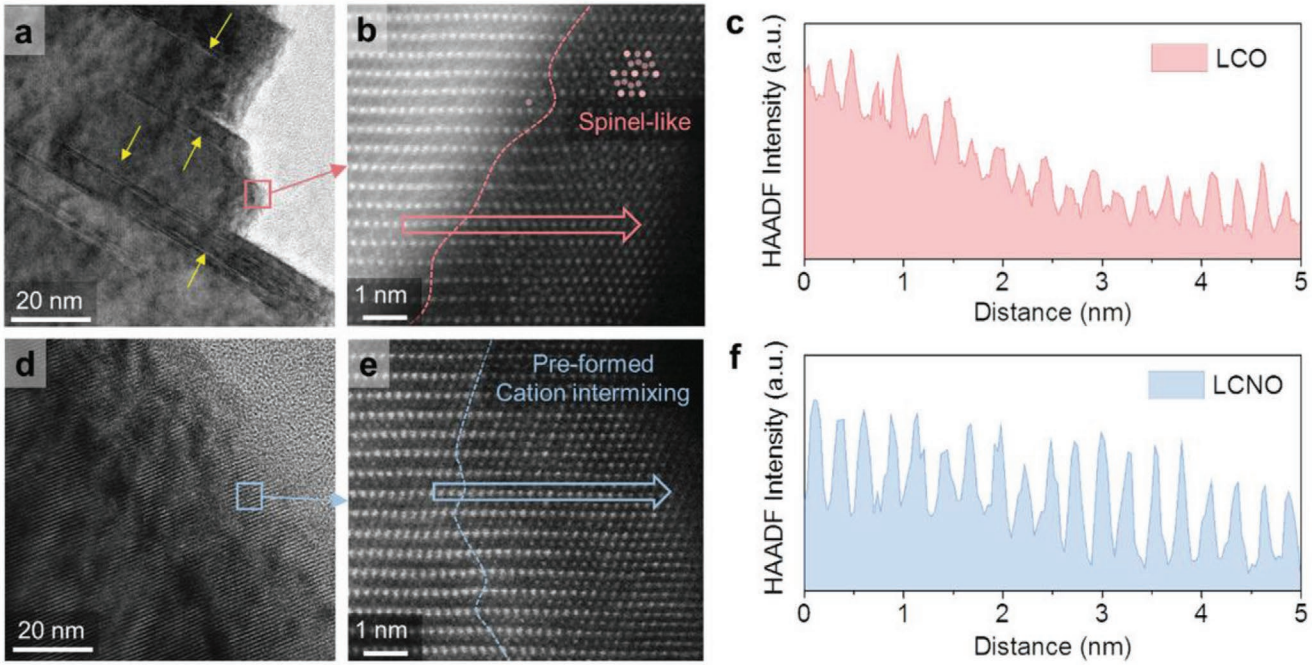

Figure 10. Surface structure of a,b) $LiCoO_2$ and d,e) $LiNi_{0.05}Co_{0.95}O_2$, and HAADF profile of c) $LiCoO_2$ and f) $LiNi_{0.05}Co_{0.95}O_2$, all cycled at 3.0–4.45 V versus Li^+/Li. Spinel-like phase forms at the surface of cycled $LiCoO_2$, while cation-mixed phase forms at the surface of $LiNi_{0.05}Co_{0.95}O_2$. Reproduced with permission.[35b] Copyright 2020, John Wiley & Sons, Inc.

© 2020 WILEY-VCH Verlag GmbH & Co. KGaA, Weinheim

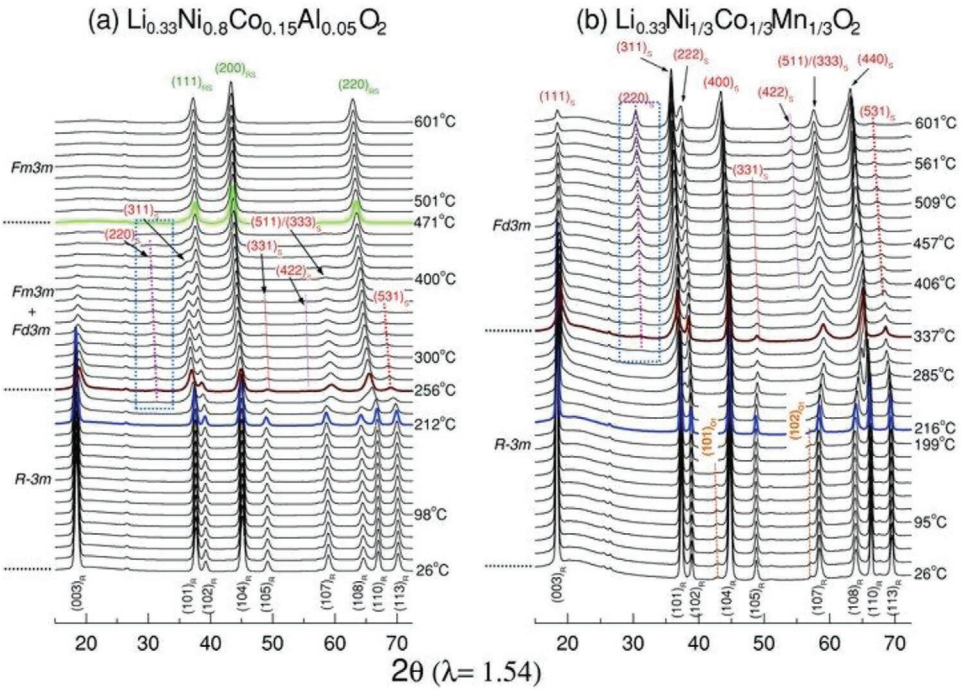

Figure 11. XRD patterns of a) $Li_{0.33}Ni_{0.8}Co_{0.15}Al_{0.05}O_2$ and b) $Li_{0.33}Ni_{1/3}Co_{1/3}Mn_{1/3}O_2$ to reveal the structural and phase evolutions during in situ heating up to 600 °C. Subscript R denotes rhombohedral layered structure ($R\bar{3}m$), S denotes spinel structure ($Fd\bar{3}m$), and RS denotes rocksalt structure ($Fm\bar{3}m$). Reproduced with permission.[104] Copyright 2013, John Wiley & Sons, Inc.

at the surface of $Li_{1.2}Ni_{0.2}Mn_{0.6}O_2$ cycled at 2.0–4.8 V versus Li^+/Li under high-resolution STEM, Gu et al.[111] observed the formation of $LiMn_2O_4$-like cubic spinel in $Li_{1.2}Ni_{0.2}Mn_{0.6}O_2$ and $Li_{1.2}Ni_{0.1}Co_{0.175}Mn_{0.525}O_2$ cycled at 2.0–4.6 V versus Li^+/Li (after three formation cycles at 2.0–4.8 V vs Li^+/Li) under TEM, Zheng et al.[112] observed the formation of spinel-like phase at the surface of $Li_{1.2}Ni_{0.2}Mn_{0.6}O_2$ cycled at 2.0–4.8 V versus Li^+/Li under STEM, and Yan et al.[113] observed the formation of $LiMn_2O_4$-type or M_3O_4-type (M: transition metal) spinel (**Figure 12**) in $Li_{1.2}Ni_{0.2}Mn_{0.6}O_2$ cycled at 2.0–4.7 V versus Li^+/Li under STEM. Interestingly, Yan et al.[114] observed the formation of spinel-like structure as well as a large population of nanovoids not only at the surface but also in the bulk of $Li_{1.2}Ni_{0.2}Mn_{0.6}O_2$ cycled at 2.0–4.8 V versus Li^+/Li by STEM-HAADF. Therefore, it is clear that spinel structure also serves as a degradation product of layered Li-rich cathodes.

The above observations in layered $LiCoO_2$, NCM, NCA, and Li-rich cathodes raise an interesting question: what is the atomistic process and the driving force for the transformation of layered structures to spinel-like structures (either good or bad) upon electrochemical cycling? There could be several possible reasons. First of all, considering the structural relationship between layered and spinel structures shown in Figures 2 and **13**,[115] TM ion migration from TM layer to Li layer is clearly involved, which could be both thermodynamically and kinetically more favorable at highly charged (i.e., delithiated) states than at discharged (i.e., stoichiometric) states. Second, the "layeredness" (i.e., cation ordering with alternating (111) planes of TM layers and Li layers) is driven by the difference in the charge and size between TM ions and Li^+. For example, Co being +3 valence and much smaller than Li^+ promotes planar Li–TM–Li–TM concentration wave in $LiCoO_2$, maintained even at high temperatures of >1000 °C in air; in comparison, Ni being only +2 valence and similar in size with Li^+ tends to cation-mix with Li^+, which sets strict requirements on the synthesis conditions (temperature and atmosphere) of $LiNiO_2$ and Ni-rich NCM/NCA. Therefore, since TM ions typically become more reduced at the surface of cycled cathodes due to anion-redox-induced oxygen mobility and oxygen loss,[32] the layeredness is difficult to maintain, which justifies why TM ions migrate into the Li layer (almost empty in highly charged states). Third, electrostatic repulsion between TM ions would tend to separate them apart, maximizing their distances and offering a driving force for cation ordering into a spinel-like pattern. (Remember in the spinel structure, B-site cations only occupy half of the octahedral sites in an edge-sharing manner.) Finally, some reduced cations such as Co^{2+} and Mn^{3+} may prefer tetrahedral sites (Co^{2+}: $e_g^4t_{2g}^3$, Mn^{3+}: $e_g^4t_{2g}^0$), which also promotes the formation of the "bad spinel" structures (there is no cation tetrahedral occupancy in layered structures). Nevertheless, in addition to the above general considerations, the detailed mechanism and kinetics of the phase transformation could vary with different materials and testing conditions (such as voltage, time, temperature, and the type of electrolytes), which are worthwhile for future investigations.

On the other hand, the robustness of the spinel structure inspires people to integrate it with other structures to improve structural stability. One such effort is to integrate the "good spinel" structure with a layered one to prepare a "composite" electrode, such as $x LiNi_{0.5}Mn_{1.5}O_4 \bullet (1-x)[Li_2MnO_3 \bullet LiNi_{0.5}Mn_{0.5}O_2]$ and $x Li_2MnO_3 \bullet (1-x) Li_{1+\delta}Mn_{2-\delta}O_4$ ($0 \le \delta \le 1/3$).[13c,116] Another commonly practiced method is to coat a stable spinel structure

© 2020 WILEY-VCH Verlag GmbH & Co. KGaA, Weinheim

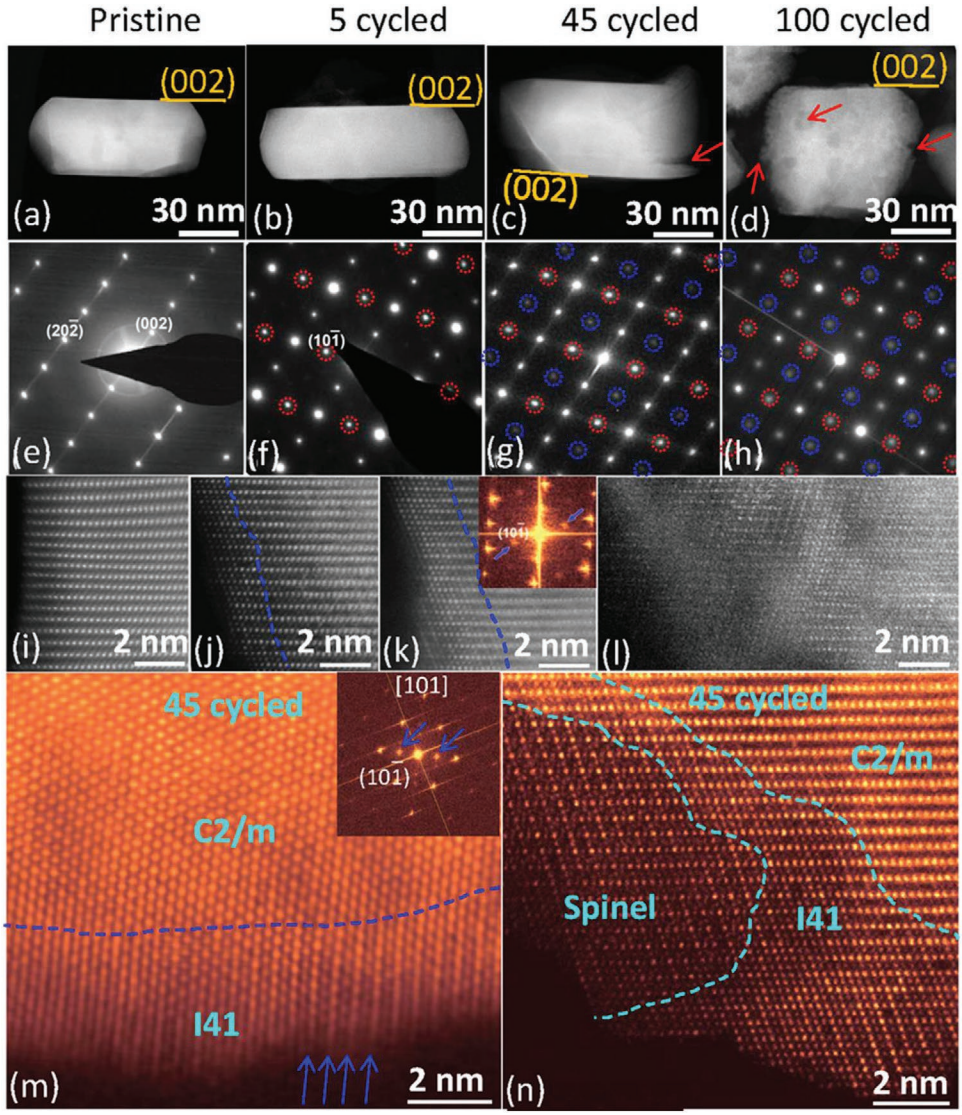

Figure 12. a–d) Low-magnification STEM-HAADF images and e–h) SAED pattern along the [010] zone axis of $Li_{1.2}Ni_{0.2}Mn_{0.6}O_2$ cycled under various conditions. i–l) High-resolution HAADF-STEM images for the surfaces of cycled particles. m,n) [010] zone axis HAADF-STEM images identified spinel structure and I41 structure in 45 cycled samples. Reproduced with permission.[113] Copyright 2014, American Chemical Society.

over high energy density cathodes such as $LiCoO_2$, high-Ni NCM/NCA, and Li-/Mn-rich materials. For example, spinel-$Li(Ni_{0.31}Co_{0.11}Mn_{0.58})_2O_4$-coated $Li(Ni_{0.54}Co_{0.12}Mn_{0.34})O_2$, spinel-$LiMn_2O_4$-coated $Li_{1.2}Mn_{0.6}Ni_{0.2}O_2$, spinel-$Li_xCo_2O_4$-coated $LiCoO_2$, spinel-$LiMn_{1.9}Al_{0.1}O_4$-coated $Li(Ni_{0.7}Co_{0.15}Mn_{0.15})O_2$, and spinel-$Li_{4/3}Mn_{5/3}O_4$-coated $Li_{1.214}Mn_{0.53}Co_{0.128}Ni_{0.128}O_2$ have been reported in the literature,[117] which demonstrate superior cycling stability over the uncoated materials. Herein, special attention should be paid to Mn^{4+}-based spinels including the well-known compositions of $Li_{4/3}Mn_{5/3}O_4$ and $LiNi_{0.5}Mn_{1.5}O_4$ as well as hypothetical ones of $xLi_{4/3}Mn_{5/3}O_4$•$(1-x)LiNi_{0.5}Mn_{1.5}O_4$ and $xLi_{4/3}Mn_{5/3}O_4$•$(1-x)LiAlMnO_4$, because they will not suffer from the damaging disproportionation reaction and Mn^{4+} is relatively catalytically inactive compared to other widely used TM ions (e.g., $Co^{3+/4+}$ and $Ni^{3+/4+}$) in LIB cathodes. Zhang et al.[117e] successfully coated a uniform layer of $Li_4Mn_5O_{12}$ on Li-rich $Li_{1.2}Mn_{0.54}Co_{0.13}Ni_{0.13}O_2$, from which they obtained better capacity and voltage retention, reduced oxygen evolution, and mitigated "bad spinel-"like phase transformation. Zhu et al.[17] coated ≈10 mm $LiCoO_2$ single crystals with a lattice-coherent $LiMn_{0.75}Ni_{0.25}O_2$ surface layer (**Figure 14**a), which normally is not stable as a bulk layered phase, but is stabilized here as an epitaxial nanolayer to the $LiCoO_2$ single crystal. This layered $LiMn_{0.75}Ni_{0.25}O_2$ further transforms into a "good" (i.e., with percolating Li^+ diffusion channels) $LiMn_{1.5}Ni_{0.5}O_4$ spinel shell during the initial electrochemical cycles that completely wetted and wrapped the $LiCoO_2$ bulk (Figure 14b). The robust "good spinel" shell effectively prevented O_2 escape and Co dissolution, which drastically improved the cyclability of $LiCoO_2$ under high voltage cycling (3.0–4.6 V vs Li^+/Li). Such novel spinel coatings are worthwhile to be further explored, probably assisted by innovative synthesis methods[32] that lead to more uniform conformal coating with better bonding to the host material.

© 2020 WILEY-VCH Verlag GmbH & Co. KGaA, Weinheim

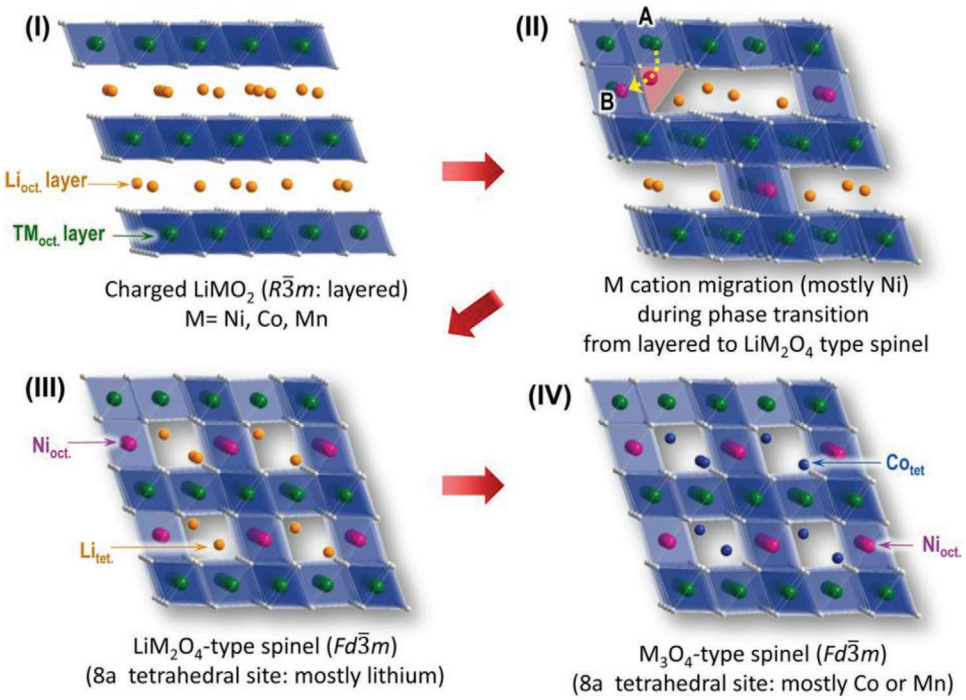

Figure 13. Schematics illustrating cation migration and structure reconstruction from I) perfect layered structure, to II) partially cation-mixed layered structure, to III) $LiMn_2O_4$-type "good" spinel structure and to IV) M_3O_4-type "bad" spinel structure. M denotes transition metal elements. The process was originally summarized for structural evolution during heat treatment, but it could be also applicable for evolution during electrochemical cycling. Reproduced with permission.[115] Copyright 2014, American Chemical Society.

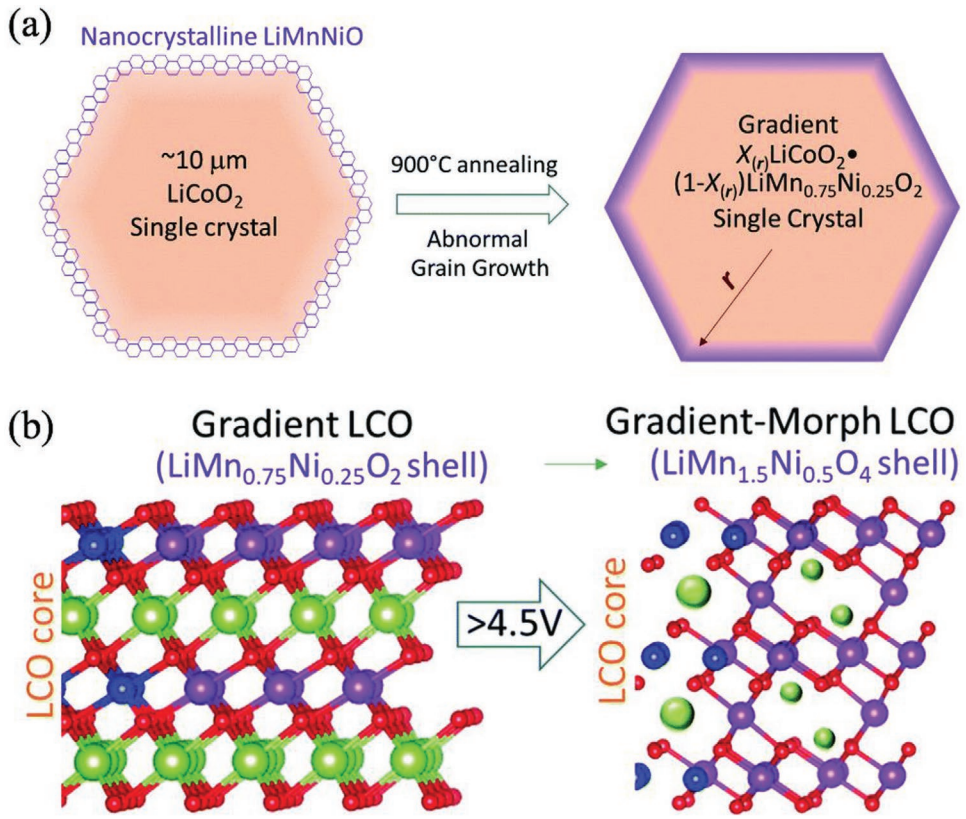

Figure 14. a) Schematic of gradient $LiCoO_2$–$LiMn_{0.75}Ni_{0.25}O_2$ single crystal created by high temperature annealing. b) Formation of semicoherent $LiMn_{1.5}Ni_{0.5}O_4$ shell on $LiCoO_2$ during initial electrochemical cycling, as the Mn:Ni:O ratio of 3:1:8 stays unchanged upon delithiation. Reproduced with permission.[17] Copyright 2020, Royal Society of Chemistry.

 © 2020 WILEY-VCH Verlag GmbH & Co. KGaA, Weinheim

Generally, if surface phase reconstruction has to happen, it is important to promote surface reconstruction to the "good spinel" phase $Li(TM)_2O_4$ instead of "bad spinel" surface phases like $(TM)_3O_4$. The defining characteristics of the "bad spinel" surface phase is the higher TM:O ratio (likely due to previous oxygen escape when charged to high voltages) and lower average valence of TM (lower than 3+). Such "bad spinel" a) is more soluble in the liquid electrolyte than "good spinel," and b) has TM packed in the tetrahedral sites in addition to the octahedral sites due to crowding, thus blocking Li^+ diffusion paths. As a rule of thumb, "bad spinel" has TM:O ratio greater than 0.5 (as in the case of Co_3O_4 and Mn_3O_4), whereas the "good spinel" has TM:O ratio equal to or less than 0.5. In the Figure 14 example, the Mn:Ni:O ratio of 3:1:8 managed to stay unchanged before and after electrochemical lithiation, and the coating stayed conformal due to prepositioning of the Mn:Ni:O elements in the correct ratio to reconstruct into arguably the best spinel possible ($LiMn_{1.5}Ni_{0.5}O_4$), with very little oxygen loss.

6. Spinel Framework for High-Rate and High-Power-Density Batteries

"Good" cubic spinels $Li(TM)_2O_4$ are known for their 3D interconnected diffusion channels, which offer isotropic pathways for fast Li^+ intercalation and enable applications in high-rate and high-power-density batteries. For spinel cathodes, both $LiMn_2O_4$ and $LiNi_{0.5}Mn_{1.5}O_4$ follow a solid-solution behavior during electrochemical cycling and their charge/discharge kinetics are controlled by Li^+ bulk diffusion. From an atomistic point of view, Li^+ diffusion takes place by a Li-vacancy-mediated hopping mechanism between two neighboring 8a tetrahedral sites, through an unoccupied 16c octahedral site that face-shares with the two tetrahedra.[118] Li^+ diffusivity of $LiMn_2O_4$ and $LiNi_{0.5}Mn_{1.5}O_4$ is experimentally measured to be in the range of 10^{-12}–10^{-9} $cm^2\ s^{-1}$, by various techniques including galvanostatic intermittent titration technique, potentiostatic intermittent titration technique, electrochemical impedance spectroscopy, electrochemical voltage spectroscopy, and current pulse relaxation.[119] According to the random-walk diffusion model, $(\text{diffusion distance})^2 = 6 \times (\text{diffusivity}) \times (\text{time})$, such a diffusivity would ensure 1 µm particles to be charged/discharged within 3–100 s, which indicates good rate capability, and allows the usage of micrometer-sized particles to be used in high-rate applications with high (volumetric) energy/power density.[120] Nanomaterials with shorter diffusion distance could enable even better kinetics at the cost of packing density and stability, and well-designed hierarchical structures could benefit from both nano- and micrometer length scales. For example, Lee et al.[121] synthesized agglomerated composite cathodes with nanosized Li-/Al-doped $LiMn_2O_4$ and well-dispersed carbon black in secondary particles (**Figure 15**), which have superior high-rate performance of 101 mAh g^{-1} under 300 C at 24 °C, and 75 mAh g^{-1} under 100 C at –10 °C. Nevertheless, the practical application of spinel cathodes in high-rate LIBs is hindered by high-temperature degradation problems, which become worse under dynamic large-current-density operations. Therefore, further improvement in cycling stability is necessary to maximize the intrinsic advantages of spinel cathodes in high-rate applications, which often requires prolonged cycle life.

Another example on the anode side is spinel $Li_4Ti_5O_{12}$, which has been commercialized as high-rate anodes in LIBs.[51,122] In electrochemical cycling, Li^+ is inserted in $Li_4Ti_5O_{12}$ to trigger a spinel-to-rocksalt conversion reaction, which is charge-compensated by Ti^{4+}/Ti^{3+} redox and offers a voltage plateau at around 1.5 V (vs Li^+/Li). Even though such a conversion reaction has sluggish kinetics in micrometer-sized $Li_4Ti_5O_{12}$, it turns out to be extremely fast in nano-$Li_4Ti_5O_{12}$.[123] Recently, through real-time characterizations of Li^+ diffusion kinetics by in situ EELS and DFT calculations, Zhang et al.[124] rationalized the facile kinetics by polyhedral distortion and high-energy metastable intermediates (well above the ground state) at the two-phase boundaries, which is not accessible by the two end members of $Li_4Ti_5O_{12}$ and $Li_7Ti_5O_{12}$ (the lithiation product). This interface-mediated diffusion kinetics were also observed by Wang et al.[123] in multiphase lithium titanate hydrates (**Figure 16**), which were able to stably deliver 130 mAh g^{-1} at ≈35 C over 10 000 cycles. The characteristic of fast kinetics together with superior cycling stability and safety offered by the robust spinel framework makes $Li_4Ti_5O_{12}$ one of the best high-rate anodes in LIBs.

The above spinel candidates as high-rate LIB cathodes/anodes make it worthwhile to think about the mechanistic reason and effective utilization of the beneficial spinel framework for Li^+ diffusion, which was laid out by a thoughtful analysis given by Urban et al.[125] Generally speaking, the macroscopic Li^+ bulk diffusion in battery electrodes is enabled by globally continuous or percolating diffusion pathways, and

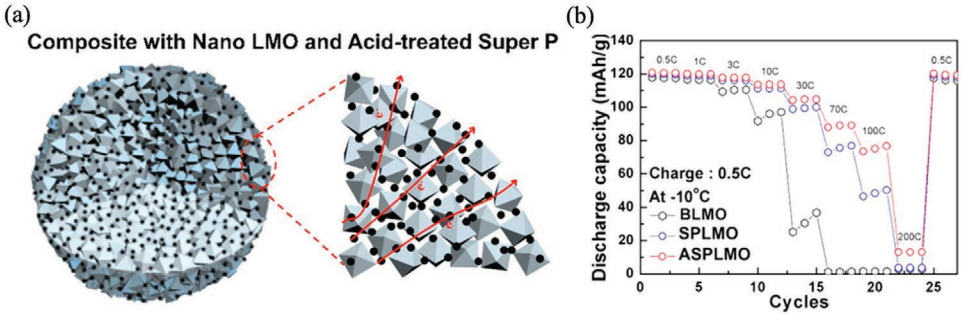

Figure 15. a) Cross-section of nanosized $Li_{1.015}Al_{0.06}Mn_{1.925}O_4$ (LMO) and acid-treated Super P composite (left), and electron percolation path (right). b) Discharge rate performance of electrodes at –10 °C (half cells, 3.0–4.5 V, BLMO: Ball-milled LMO, SPLMO: nano-LMO and Super P composite, ASPLMO: nano-LMO and acid-treated Super P composite). Reproduced with permission.[121] Copyright 2017, American Chemical Society.

© 2020 WILEY-VCH Verlag GmbH & Co. KGaA, Weinheim

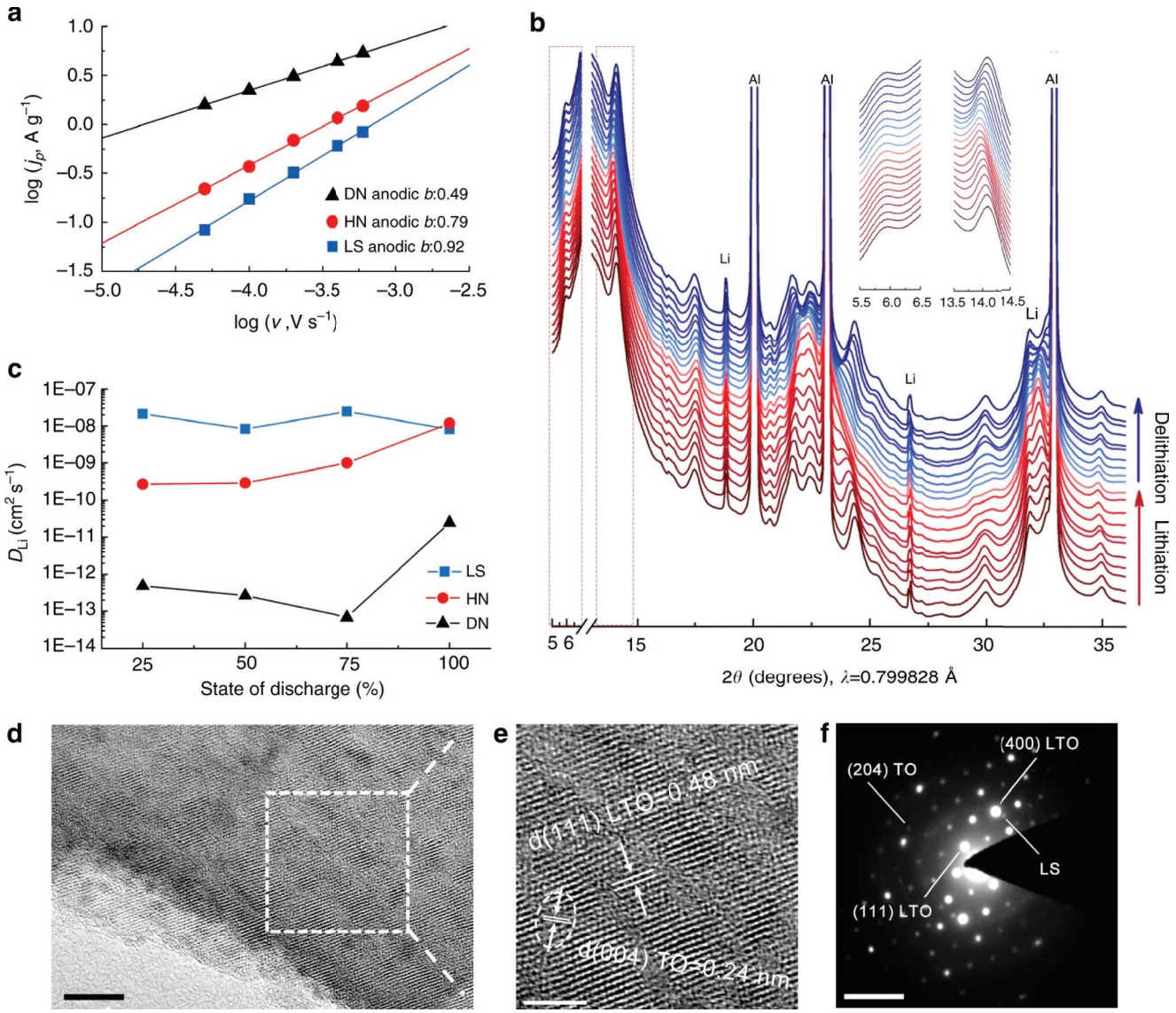

Figure 16. a) *b*-value analysis and c) calculated Li^+ diffusivity of three multiphase lithium titanate hydrate composites: a hydrated nanocomposite (HN), a low-temperature treated layered-structure nanocomposite (LS), and a high-temperature treated dried nanocomposite (DN). b) In situ synchrotron XRD of LS electrode cycled at 100 mA g^{-1}. d) HRTEM image and f) SAED pattern of HN sample. e) Magnified regime of (d) showing $Li_4Ti_5O_{12}$-like and TiO_2-like phases. Reproduced with permission.[123] Copyright 2017, Springer Nature.

locally, it is rate-limited by the available hopping path with the lowest energy barrier. On one hand, the "good spinel" structure has no problem in terms of global diffusion, because of the 3D connected diffusion channel schematically plotted in Figure 2b. Locally, Urban et al. offered a model to correlate the Li^+ diffusion barrier with the number of neighboring octahedral TM ions for the saddle-point tetrahedral Li^+ in rocksalt-based structure (recall that layered structure can be viewed as a cation-ordered rocksalt structure). This model is based on the critical role of Coulombic repulsion between Li^+ and TM ions, which peaks when the Li^+ is at the saddle point of the migration pathway (i.e., tetrahedral site in the rocksalt structure) due to very short Li–TM distance. Note that the distance between neighboring face-sharing octahedral and tetrahedral sites is much shorter than the distance between neighboring edge-sharing octahedral and octahedral sites. Therefore, Li^+ with the least (i.e., zero) neighboring TM ions should have the smallest migration barrier, and a percolating network by the so-called 0-TM Li^+ is responsible for the long-range diffusion in Li-rich disordered rocksalt cathodes.[16g] This model can be generalized to the spinel structure, where the saddle-point octahedral Li^+ is only in contact with TM-empty face-sharing tetrahedral sites. In this sense, Li^+ migration in the spinel structure always takes place by 0-TM mode, which rationalizes the origin of its fast diffusion kinetics. In the spinel-like low-temperature $LiCoO_2$ structure (similar structure to the lithiated spinel or tetragonal rocksalt $Li_2Mn_2O_4$, where Co ordering in the cation sublattice is the same as the Mn pattern in $LiMn_2O_4$), 0-TM mode is also available, which could help enhance diffusion kinetics. Such local structure with partial spinel-like

© 2020 WILEY-VCH Verlag GmbH & Co. KGaA, Weinheim

order has been recently demonstrated by Ji et al.[15b] in Li-rich oxyfluorides with compositions of $Li_{1.68}Mn_{1.6}O_{3.7}F_{0.3}$ and $Li_{1.68}Mn_{1.6}O_{3.4}F_{0.6}$. The oxyfluorides are cycled on combined cationic and anionic redox and show excellent electrochemical performance with high capacity of >360 mAh g^{-1}, high energy density of >1100 Wh kg^{-1}, and ultrafast rate capability up to 20 000 mA g^{-1} when cycled between 1.5 and 4.8 V (vs Li^+/Li). This highlights the great promise of utilizing spinel and spinel-like structures to design novel high-rate cathode materials, as well as engineered cationic and anionic redox activities.[126]

7. Conclusion and Remarks

To summarize, the fundamental understanding of spinel $LiMn_2O_4$ cathode and its derivatives were reviewed in this article, which provide valuable insights for the future development of LIB cathodes. With advantages especially in low cost, good thermal stability, high rate capability, and ease of synthesis, the optimized spinel cathodes such as $LiMn_2O_4$ and $LiNi_{0.5}Mn_{1.5}O_4$ are promising in future applications of energy storage systems, power tools, and electric vehicles.

We believe the following aspects are of central importance in spinel and related cathodes:

1) More fundamental studies should be conducted to better understand the degradation mechanisms of spinel cathodes, especially the main problems of TM dissolution and surface/interface instability. Such knowledge should be transferable to other electrode materials, especially Mn-containing ones.
2) Further development of spinel cathodes relies on optimizations on bulk doping, control of dopant distribution, coating, liquid electrolytes, and potential applications in all-solid-state batteries. Special attention to surface doping and development of new liquid electrolytes are recommended. Machine learning and robotic synthesis could potentially be helpful in optimizations in the hyperspace of compositions and various processing parameters.
3) Spinel structures can be integrated in the bulk and/or at the surface of other high-capacity cathode materials, especially the layered cathodes that share the same oxygen sublattice. Special attention should be paid to the elements and valence of the spinel stabilizer, whereas catalytically active TM ions should be avoided. More fundamental studies are suggested to understand the phase evolution and transformation dynamics at the surface of high-capacity cathodes, preferentially under dynamic conditions, to guide the reconstruction toward "good spinel" surface phases with percolating Li conduction pathways, instead of "bad spinel" surface phases where such pathways are blocked by TMs. As a rule of thumb, "bad spinel" has TM:O ratio greater than 0.5 (as in the case of Co_3O_4 and Mn_3O_4), likely due to oxygen loss in electrochemical cycling, whereas the "good spinel" has TM:O ratio equal to or less than 0.5. For instance, $LiMn_2O_4$ spinel is obviously a "good spinel," but with cycling, this spinel is naturally subjected to a certain degree of surface oxygen loss, which in turn leads to the gradual formation of the "bad" Mn_3O_4 spinel. "Bad spinels" are bad because they are more soluble in the liquid electrolyte due to lower TM valence (less than 3+), and they also block Li diffusion paths and greatly increase the impedance, with TMs sitting at tetrahedral sites in addition to octahedral sites. If the cathode surface has to reconstruct, being able to distinguish the "good spinel" from the "bad spinel" surface phases, and guiding the reconstruction toward a "good spinel," would be key.
4) Spinel structures and rocksalt structures with spinel-like order could be beneficially used to design new cathode materials for high-energy-density applications. To simultaneously increase the capacity, Li-excess compositions should be explored with activated anion redox. The fundamental mechanisms of fast kinetics and reversible hybrid anion- and cation-redox mechanisms in spinel-like structures are worthwhile for detailed investigations in the future.

Acknowledgements

Y.H. and Y.D. contributed equally to this work. The authors acknowledge support by the Department of Energy, Basic Energy Sciences, under Award Number DE-SC0002633 (Chemomechanics of Far-From-Equilibrium Interfaces), and the U.S. Department of Energy (USDOE), Office of Energy Efficiency and Renewable Energy (EERE), Advanced Manufacturing Office (AMO) R&D Projects Emerging Research Exploration, under DOE Idaho Operations Office with Contract No. DE-AC07-05ID14517.

Conflict of Interest

The authors declare no conflict of interest.

Keywords

bad spinel, HACR, Li-rich spinel, Mn dissolution, spinel-like

Received: March 17, 2020
Revised: April 30, 2020
Published online:

[1] NobelPrize.org, The Nobel Prize in Chemistry **2019**, https://www.ncbi.nlm.nih.gov/pubmed/28931813 (accessed: February 2020).
[2] K. Mizushima, P. C. Jones, P. J. Wiseman, J. B. Goodenough, *Mater. Res. Bull.* **1980**, *15*, 783.
[3] a) M. M. Thackeray, W. I. F. David, P. G. Bruce, J. B. Goodenough, *Mater. Res. Bull.* **1983**, *18*, 461; b) M. M. Thackeray, P. J. Johnson, L. A. Depicciotto, P. G. Bruce, J. B. Goodenough, *Mater. Res. Bull.* **1984**, *19*, 179.
[4] A. K. Padhi, K. S. Nanjundaswamy, J. B. Goodenough, *J. Electrochem. Soc.* **1997**, *144*, 1188.
[5] J. B. Goodenough, *J. Power Sources* **2007**, *174*, 996.
[6] J. C. Hunter, *J. Solid State Chem.* **1981**, *39*, 142.
[7] M. M. Thackeray, W. I. F. David, J. B. Goodenough, *Mater. Res. Bull.* **1982**, *17*, 785.
[8] a) Y. Y. Xia, M. Yoshio, *J. Electrochem. Soc.* **1996**, *143*, 825; b) G. Pistoia, D. Zane, Y. Zhang, *J. Electrochem. Soc.* **1995**, *142*, 2551; c) J. Sugiyama, T. Atsumi, T. Hioki, S. Noda, N. Kamegashira, *J. Alloys Compd.* **1996**, *235*, 163; d) J. M. Tarascon, W. R. Mckinnon,

 © 2020 WILEY-VCH Verlag GmbH & Co. KGaA, Weinheim

F. Coowar, T. N. Bowmer, G. Amatucci, D. Guyomard, *J. Electrochem. Soc.* **1994**, *141*, 1421; e) D. Guyomard, J. M. Tarascon, *Solid State Ionics* **1994**, *69*, 222; f) G. G. Amatucci, A. Blyr, C. Sigala, P. Alfonse, J. M. Tarascon, *Solid State Ionics* **1997**, *104*, 13; g) A. Du Pasquier, A. Blyr, P. Courjal, D. Larcher, G. Amatucci, B. Gerand, J. M. Tarascon, *J. Electrochem. Soc.* **1999**, *146*, 428; h) G. Amatucci, A. Du Pasquier, A. Blyr, T. Zheng, J. M. Tarascon, *Electrochim. Acta* **1999**, *45*, 255; i) J. Cho, M. M. Thackeray, *J. Electrochem. Soc.* **1999**, *146*, 3577.

[9] a) M. M. Thackeray, A. Dekock, M. H. Rossouw, D. Liles, R. Bittihn, D. Hoge, *J. Electrochem. Soc.* **1992**, *139*, 363; b) M. M. Thackeray, *Prog. Solid State Chem.* **1997**, *25*, 1.

[10] R. J. Gummow, A. Dekock, M. M. Thackeray, *Solid State Ionics* **1994**, *69*, 59.

[11] a) Q. M. Zhong, A. Bonakdarpour, M. J. Zhang, Y. Gao, J. R. Dahn, *J. Electrochem. Soc.* **1997**, *144*, 205; b) K. Amine, H. Tukamoto, H. Yasuda, Y. Fujita, *J. Power Sources* **1997**, *68*, 604; c) A. Manthiram, K. Chemelewski, E. S. Lee, *Energy Environ. Sci.* **2014**, *7*, 1339.

[12] a) M. H. Rossouw, D. C. Liles, M. M. Thackeray, *J. Solid State Chem.* **1993**, *104*, 464; b) P. Kalyani, S. Chitra, T. Mohan, S. Gopukumar, *J. Power Sources* **1999**, *80*, 103; c) A. Manthiram, J. C. Knight, S. T. Myung, S. M. Oh, Y. K. Sun, *Adv. Energy Mater.* **2016**, *6*, 1501010; d) J. M. Zheng, S. J. Myeong, W. R. Cho, P. F. Yan, J. Xiao, C. M. Wang, J. Cho, J. G. Zhang, *Adv. Energy Mater.* **2017**, *7*, 1601284.

[13] a) A. R. Armstrong, P. G. Bruce, *Nature* **1996**, *381*, 499; b) C. S. Johnson, N. Li, J. T. Vaughey, S. A. Hackney, M. M. Thackeray, *Electrochem. Commun.* **2005**, *7*, 528; c) M. M. Thackeray, C. S. Johnson, J. T. Vaughey, N. Li, S. A. Hackney, *J. Mater. Chem.* **2005**, *15*, 2257.

[14] R. Schmuch, R. Wagner, G. Horpel, T. Placke, M. Winter, *Nat. Energy* **2018**, *3*, 267.

[15] a) J. M. Tarascon, E. Wang, F. K. Shokoohi, W. R. Mckinnon, S. Colson, *J. Electrochem. Soc.* **1991**, *138*, 2859; b) H. Ji, J. Wu, Z. Cai, J. Liu, D.-H. Kwon, H. Kim, A. Urban, J. K. Papp, E. Foley, Y. Tian, M. Balasubramanian, H. Kim, R. J. Clément, B. D. McCloskey, W. Yang, G. Ceder, *Nat. Energy* **2020**, *5*, 213.

[16] a) J. R. Dahn, U. Vonsacken, C. A. Michal, *Solid State Ionics* **1990**, *44*, 87; b) E. Rossen, C. D. W. Jones, J. R. Dahn, *Solid State Ionics* **1992**, *57*, 311; c) E. Zhecheva, R. Stoyanova, *Solid State Ionics* **1993**, *66*, 143; d) M. Yoshio, H. Noguchi, J. Itoh, M. Okada, T. Mouri, *J. Power Sources* **2000**, *90*, 176; e) J. S. Weaving, F. Coowar, D. A. Teagle, J. Cullen, V. Dass, P. Bindin, R. Green, W. J. Macklin, *J. Power Sources* **2001**, *97–98*, 733; f) Z. H. Lu, D. D. MacNeil, J. R. Dahn, *Electrochem. Solid-State Lett.* **2001**, *4*, A191; g) J. Lee, A. Urban, X. Li, D. Su, G. Hautier, G. Ceder, *Science* **2014**, *343*, 519.

[17] Z. Zhu, D. Yu, Z. Shi, R. Gao, X. Xiao, I. Waluyo, M. Ge, Y. Dong, W. Xue, G. Xu, W.-K. Lee, A. Hunt, J. Li, *Energy Environ. Sci.* **2020**, https://doi.org/10.1039/d0ee00231c.

[18] M. J. Lee, S. Lee, P. Oh, Y. Kim, J. Cho, *Nano Lett.* **2014**, *14*, 993.

[19] T. F. Yi, J. Mei, Y. R. Zhu, *J. Power Sources* **2016**, *316*, 85.

[20] N. Xu, H. B. Zhou, Y. H. Liao, G. J. Li, M. Q. Xu, W. S. Li, *Solid State Ionics* **2019**, *341*, 115049.

[21] a) P. He, H. R. Wang, L. Qi, T. Osaka, *J. Power Sources* **2006**, *160*, 627; b) H. J. Noh, S. Youn, C. S. Yoon, Y. K. Sun, *J. Power Sources* **2013**, *233*, 121.

[22] L. W. Liang, G. R. Hu, F. Jiang, Y. B. Cao, *J. Alloys Compd.* **2016**, *657*, 570.

[23] N. T. Wu, H. Wu, W. Yuan, S. J. Liu, J. Y. Liao, Y. Zhang, *J. Mater. Chem. A* **2015**, *3*, 13648.

[24] a) F. He, X. Q. Wang, C. Q. Du, A. P. Baker, J. W. Wu, X. H. Zhang, *Electrochim. Acta* **2015**, *153*, 484; b) B. Qiu, J. Wang, Y. G. Xia, Y. Z. Liu, L. F. Qin, X. Y. Yao, Z. P. Liu, *J. Power Sources* **2013**, *240*, 530; c) L. Ku, Y. X. Cai, Y. T. Ma, H. F. Zheng, P. F. Liu, Z. S. Qiao, Q. S. Xie, L. S. Wang, D. L. Peng, *Chem. Eng. J.* **2019**, *370*, 499.

[25] W. J. Zhang, *J. Power Sources* **2011**, *196*, 2962.

[26] S. K. Martha, J. Grinblat, O. Haik, E. Zinigrad, T. Drezen, J. H. Miners, I. Exnar, A. Kay, B. Markovsky, D. Aurbach, *Angew. Chem., Int. Ed.* **2009**, *48*, 8559.

[27] J. B. Goodenough, K. S. Park, *J. Am. Chem. Soc.* **2013**, *135*, 1167.

[28] R. A. House, P. G. Bruce, *Nat. Energy* **2020**, *5*, 191.

[29] M. D. Radin, S. Hy, M. Sina, C. C. Fang, H. D. Liu, J. Vinckeviciute, M. H. Zhang, M. S. Whittingham, Y. S. Meng, A. Van der Ven, *Adv. Energy Mater.* **2017**, *7*, 1602888.

[30] a) M. M. Thackeray, J. R. Croy, E. Lee, A. Gutierrez, M. N. He, J. S. Park, B. T. Yonemoto, B. R. Long, J. D. Blauwkamp, C. S. Johnson, Y. Shin, W. I. F. David, *Sustainable Energy Fuels* **2018**, *2*, 1375; b) C. Masquelier, M. Tabuchi, K. Ado, R. Kanno, Y. Kobayashi, Y. Maki, O. Nakamura, J. B. Goodenough, *J. Solid State Chem.* **1996**, *123*, 255; c) J. M. Paulsen, J. R. Dahn, *Chem. Mater.* **1999**, *11*, 3065.

[31] Y. Liu, G. Liu, H. Xu, Y. H. Zheng, Y. H. Huang, S. Li, J. Li, *Chem. Commun.* **2019**, *55*, 8118.

[32] Z. Zhu, D. W. Yu, Y. Yang, C. Su, Y. M. Huang, Y. H. Dong, I. Waluyo, B. M. Wang, A. Hunt, X. H. Yao, J. Lee, W. J. Xue, J. Li, *Nat. Energy* **2019**, *4*, 1049.

[33] R. J. Gummow, D. C. Liles, M. M. Thackeray, *Mater. Res. Bull.* **1993**, *28*, 1249.

[34] a) E. Peled, *J. Electrochem. Soc.* **1979**, *126*, 2047; b) M. Winter, B. Barnett, K. Xu, *Chem. Rev.* **2018**, *118*, 11433.

[35] a) R. Robert, C. Bunzli, E. J. Berg, P. Novak, *Chem. Mater.* **2015**, *27*, 526; b) M. Yoon, Y. Dong, Y. Yoo, S. Myeong, J. Hwang, J. Kim, S. H. Choi, J. Sung, S. J. Kang, J. Li, J. Cho, *Adv. Funct. Mater.* **2020**, *30*, 1907903; c) K. Luo, M. R. Roberts, R. Hao, N. Guerrini, D. M. Pickup, Y. S. Liu, K. Edstrom, J. H. Guo, A. V. Chadwick, L. C. Duda, P. G. Bruce, *Nat. Chem.* **2016**, *8*, 684.

[36] a) C. Zhan, T. P. Wu, J. Lu, K. Amine, *Energy Environ. Sci.* **2018**, *11*, 243; b) A. Bhandari, J. Bhattacharya, *J. Electrochem. Soc.* **2017**, *164*, A106.

[37] a) A. Blyr, C. Sigala, G. Amatucci, D. Guyomard, Y. Chabre, J. M. Tarascon, *J. Electrochem. Soc.* **1998**, *145*, 194; b) S. Komaba, T. Itabashi, T. Ohtsuka, H. Groult, N. Kumagai, B. Kaplan, H. Yashiro, *J. Electrochem. Soc.* **2005**, *152*, A937.

[38] D. P. Abraham, T. Spila, M. M. Furczon, E. Sammann, *Electrochem. Solid-State Lett.* **2008**, *11*, A226.

[39] S. R. Gowda, K. G. Gallagher, J. R. Croy, M. Bettge, M. M. Thackeray, M. Balasubramanian, *Phys. Chem. Chem. Phys.* **2014**, *16*, 6898.

[40] N. P. W. Pieczonka, Z. Y. Liu, P. Lu, K. L. Olson, J. Moote, B. R. Powell, J. H. Kim, *J. Phys. Chem. C* **2013**, *117*, 15947.

[41] J. Betz, J. P. Brinkmann, R. Nolle, C. Lurenbaum, M. Kolek, M. C. Stan, M. Winter, T. Placke, *Adv. Energy Mater.* **2019**, *9*, 1900574.

[42] a) D. C. Lin, Y. Y. Liu, Y. Cui, *Nat. Nanotechnol.* **2017**, *12*, 194; b) S. Li, M. W. Jiang, Y. Xie, H. Xu, J. Y. Jia, J. Li, *Adv. Mater.* **2018**, *30*, 1706375.

[43] D. H. Jang, Y. J. Shin, S. M. Oh, *J. Electrochem. Soc.* **1996**, *143*, 2204.

[44] Y. Terada, Y. Nishiwaki, I. Nakai, F. Nishikawa, *J. Power Sources* **2001**, *97–98*, 420.

[45] a) L. F. Wang, C. C. Ou, K. A. Striebel, J. J. S. Chen, *J. Electrochem. Soc.* **2003**, *150*, A905; b) Y. Y. Xia, Y. H. Zhou, M. Yoshio, *J. Electrochem. Soc.* **1997**, *144*, 2593; c) A. Blyr, A. Du Pasquier, G. Amatucci, J. M. Tarascon, *Ionics* **1997**, *3*, 321; d) D. H. Jang, S. M. Oh, *J. Electrochem. Soc.* **1997**, *144*, 3342.

[46] a) Y. Shilina, B. Ziv, A. Meir, A. Banerjee, S. Ruthstein, S. Luski, D. Aurbach, I. C. Halalay, *Anal. Chem.* **2016**, *88*, 4440; b) A. Banerjee, Y. Shilina, B. Ziv, J. M. Ziegelbauer, S. Luski, D. Aurbach, I. C. Halalay, *J. Am. Chem. Soc.* **2017**, *139*, 1738.

[47] L. Hanf, J. Henschel, M. Diehl, M. Winter, S. Nowak, *Electrophoresis* **2020**, *41*, 697.

© 2020 WILEY-VCH Verlag GmbH & Co. KGaA, Weinheim

[48] D. C. Tang, Y. Sun, Z. Z. Yang, L. B. Ben, L. Gu, X. J. Huang, *Chem. Mater.* **2014**, *26*, 3535.
[49] X. Gao, Y. H. Ikuhara, C. A. J. Fisher, R. Huang, A. Kuwabara, H. Moriwake, K. Kohama, Y. Ikuhara, *J. Mater. Chem. A* **2019**, *7*, 8845.
[50] M. Hirayama, H. Ido, K. Kim, W. Cho, K. Tamura, J. Mizuki, R. Kanno, *J. Am. Chem. Soc.* **2010**, *132*, 15268.
[51] M. M. Thackeray, *J. Am. Ceram. Soc.* **1999**, *82*, 3347.
[52] D. Aurbach, M. D. Levi, K. Gamulski, B. Markovsky, G. Salitra, E. Levi, U. Heider, L. Heider, R. Oesten, *J. Power Sources* **1999**, *81–82*, 472.
[53] a) A. Yamada, M. Tanaka, *Mater. Res. Bull.* **1995**, *30*, 715; b) A. Yamada, M. Tanaka, K. Tanaka, K. Sekai, *J. Power Sources* **1999**, *81–82*, 73.
[54] M. M. Thackeray, Y. Shao-Horn, A. J. Kahaian, K. D. Kepler, J. T. Vaughey, S. A. Hackney, *Electrochem. Solid-State Lett.* **1999**, *1*, 7.
[55] T. C. Liu, A. Dai, J. Lu, Y. F. Yuan, Y. G. Xiao, L. Yu, M. Li, J. Gim, L. Ma, J. J. Liu, C. Zhan, L. X. Li, J. X. Zheng, Y. Ren, T. P. Wu, R. Shahbazian-Yassar, J. G. Wen, F. Pan, K. Amine, *Nat. Commun.* **2019**, *10*, 4721.
[56] M. X. Lin, L. B. Ben, Y. Sun, H. Wang, Z. Z. Yang, L. Gu, X. Q. Yu, X. Q. Yang, H. F. Zhao, R. Yu, M. Armand, X. J. Huang, *Chem. Mater.* **2015**, *27*, 292.
[57] C. D. Amos, M. A. Roldan, M. Varela, J. B. Goodenough, P. J. Ferreira, *Nano Lett.* **2016**, *16*, 2899.
[58] S. Kim, M. Aykol, C. Wolverton, *Phys. Rev. B* **2015**, *92*, 115411.
[59] Y. Y. Chen, L. B. Ben, B. Chen, W. W. Zhao, X. J. Huang, *Adv. Mater. Interfaces* **2018**, *5*, 1800077.
[60] D. W. Shin, C. A. Bridges, A. Huq, M. P. Paranthaman, A. Manthiram, *Chem. Mater.* **2012**, *24*, 3720.
[61] G. Zhou, X. Sun, Q. H. Li, X. Wang, J. N. Zhang, W. Yang, X. Yu, R. Xiao, H. Li, *J. Phys. Chem. Lett.* **2020**, *11*, 3051.
[62] a) K. Leung, *Chem. Mater.* **2017**, *29*, 2550; b) R. Benedek, M. M. Thackeray, J. Low, T. Bucko, *J. Phys. Chem. C* **2012**, *116*, 4050.
[63] a) D. Song, H. Ikuta, T. Uchida, M. Wakihara, *Solid State Ionics* **1999**, *117*, 151; b) Y. S. Lee, N. Kumada, M. Yoshio, *J. Power Sources* **2001**, *96*, 376; c) Y. Shin, A. Manthiram, *Chem. Mater.* **2003**, *15*, 2954; d) Y. J. Shin, A. Manthiram, *J. Electrochem. Soc.* **2004**, *151*, A204; e) A. Gutierrez, A. Manthiram, *J. Electrochem. Soc.* **2013**, *160*, A901; f) L. L. Xiong, Y. L. Xu, T. Tao, J. B. Goodenough, *J. Power Sources* **2012**, *199*, 214; g) S. Bhuvaneswari, U. V. Varadaraju, R. Gopalan, R. Prakash, *Electrochim. Acta* **2019**, *301*, 342.
[64] a) Y. Yu, M. W. Xiang, J. M. Guo, C. W. Su, X. F. Liu, H. L. Bai, W. Bai, K. J. Duan, *J. Colloid Interface Sci.* **2019**, *555*, 64; b) C. Ma, L. Luo, K. W. Li, B. Zhou, Q. Shi, *Int. J. Electrochem. Sci.* **2019**, *14*, 7643; c) Z. R. Yang, Y. J. Wang, X. C. Chen, H. Wu, Y. Zhang, *ChemistrySelect* **2019**, *4*, 9583.
[65] X. M. He, J. J. Li, Y. Cai, Y. W. Wang, H. R. Ying, C. Y. Jiang, C. R. Wan, *Solid State Ionics* **2005**, *176*, 2571.
[66] J. L. Shi, D. D. Xiao, M. Y. Ge, X. Q. Yu, Y. Chu, X. J. Huang, X. D. Zhang, Y. X. Yin, X. Q. Yang, Y. G. Guo, L. Gu, L. J. Wan, *Adv. Mater.* **2018**, *30*, 1705575.
[67] a) G. M. Liang, Z. B. Wu, C. Didier, W. C. Zhang, J. Cuan, B. H. Li, K. Y. Ko, P. Y. Hung, C. Z. Lu, Y. Z. Chen, G. Leniec, S. M. Kaczmarek, B. Johannessen, L. Thomsen, V. K. Peterson, W. K. Pang, Z. P. Guo, *Angew. chem., Int. Ed.* **2020**, https://doi.org/10.1002/anie.202001454; b) C. Locati, U. Lafont, L. Simonin, F. Ooms, E. M. Kelder, *J. Power Sources* **2007**, *174*, 847; c) S. R. Li, C. H. Chen, J. R. Dahn, *J. Electrochem. Soc.* **2013**, *160*, A2166; d) J. Mao, M. Z. Ma, P. P. Liu, J. H. Hu, G. S. Shao, V. Battaglia, K. H. Dai, G. Liu, *Solid State Ionics* **2016**, *292*, 70; e) M. Aklalouch, J. M. Amarilla, R. M. Rojas, I. Saadoune, J. M. Rojo, *J. Power Sources* **2008**, *185*, 501; f) G. B. Zhong, Y. Y. Wang, Z. C. Zhang, C. H. Chen, *Electrochim. Acta* **2011**, *56*, 6554; g) H. L. Wang, T. A. Tan, P. Yang, M. O. Lai, L. Lui, *J. Phys. Chem. C* **2011**, *115*, 6102.
[68] a) J. G. Yang, X. P. Han, X. L. Zhang, F. Y. Cheng, J. Chen, *Nano Res.* **2013**, *6*, 679; b) R. Santhanam, B. Rambabu, *J. Power Sources* **2010**, *195*, 5442.
[69] a) J. Lu, C. Zhan, T. P. Wu, J. G. Wen, Y. Lei, A. J. Kropf, H. M. Wu, D. J. Miller, J. W. Elam, Y. K. Sun, X. P. Qiu, K. Amine, *Nat. Commun.* **2014**, *5*, 5693; b) J. Y. Piao, Y. G. Sun, S. Y. Duan, A. M. Cao, X. L. Wang, R. J. Xiao, X. Q. Yu, Y. Gong, L. Gu, Y. T. Li, Z. J. Liu, Z. Q. Peng, R. M. Qiao, W. L. Yang, X. Q. Yang, J. B. Goodenough, L. J. Wan, *Chem* **2018**, *4*, 1685; c) J. M. Lim, R. G. Oh, D. Kim, W. Cho, K. Cho, M. Cho, M. S. Park, *ChemSusChem* **2016**, *9*, 2967; d) Y. Xue, L. L. Zheng, J. Wang, J. G. Zhou, F. D. Yu, G. J. Zhou, Z. B. Wang, *ACS Appl. Energy Mater.* **2019**, *2*, 2982; e) W. Zhang, X. L. Sun, Y. X. Tang, H. R. Xia, Y. Zeng, L. Qiao, Z. Q. Zhu, Z. S. Lv, Y. Y. Zhang, X. Ge, S. B. Xi, Z. G. Wang, Y. H. Du, X. D. Chen, *J. Am. Chem. Soc.* **2019**, *141*, 14038.
[70] a) Y. K. Sun, K. J. Hong, J. Prakash, *J. Electrochem. Soc.* **2003**, *150*, A970; b) M. M. Thackeray, C. S. Johnson, J. S. Kim, K. C. Lauzze, J. T. Vaughey, N. Dietz, D. Abraham, S. A. Hackney, W. Zeltner, M. A. Anderson, *Electrochem. Commun.* **2003**, *5*, 752; c) J. S. Kim, C. S. Johnson, J. T. Vaughey, S. A. Hackney, K. A. Walz, W. A. Zeltner, M. A. Anderson, M. M. Thackeray, *J. Electrochem. Soc.* **2004**, *151*, A1755; d) S. C. Park, Y. M. Kim, S. C. Han, S. Ahn, C. H. Ku, J. Y. Lee, *J. Power Sources* **2002**, *107*, 42.
[71] a) A. Tron, Y. D. Park, J. Mun, *J. Power Sources* **2016**, *325*, 360; b) J. N. Cao, G. S. Cao, H. M. Yu, J. A. Xie, X. B. Zhao, *Rare Met.* **2011**, *30*, 39; c) S. Zhao, Y. Bai, Q. Chang, Y. Yang, W. Zhang, *Electrochim. Acta* **2013**, *108*, 727.
[72] a) C. B. Qing, Y. Bai, J. M. Yang, W. F. Zhang, *Electrochim. Acta* **2011**, *56*, 6612; b) D. Q. Liu, Z. Z. He, X. Liu, *Mater. Lett.* **2007**, *61*, 4703.
[73] R. Zhao, L. Li, T. H. Xu, D. D. Wang, D. Pan, G. J. He, H. L. Zhao, Y. Bai, *ACS Appl. Mater. Interfaces* **2019**, *11*, 16233.
[74] R. Vidu, P. Stroeve, *Ind. Eng. Chem. Res.* **2004**, *43*, 3314.
[75] L. Li, R. Zhao, D. Pan, S. Yi, L. Gao, G. He, H. Zhao, C. Yu, Y. Bai, *J. Power Sources* **2020**, *450*, 227677.
[76] a) D. K. Kim, P. Muralidharan, H. W. Lee, R. Ruffo, Y. Yang, C. K. Chan, H. Peng, R. A. Huggins, Y. Cui, *Nano Lett.* **2008**, *8*, 3948; b) K. Zhang, X. P. Han, Z. Hu, X. L. Zhang, Z. L. Tao, J. Chen, *Chem. Soc. Rev.* **2015**, *44*, 699.
[77] a) H. Yamane, T. Inoue, M. Fujita, M. Sano, *J. Power Sources* **2001**, *99*, 60; b) K. Amine, J. Liu, S. Kang, I. Belharouak, Y. Hyung, D. Vissers, G. Henriksen, *J. Power Sources* **2004**, *129*, 14; c) S. S. Zhang, *J. Power Sources* **2006**, *162*, 1379; d) S. S. Zhang, K. Xu, T. R. Jow, *J. Solid State Electrochem.* **2003**, *7*, 492; e) A. Banerjee, B. Ziv, Y. Shilina, S. Luski, D. Aurbach, I. C. Halalay, *ACS Energy Lett.* **2017**, *2*, 2388.
[78] a) L. M. Suo, O. Borodin, T. Gao, M. Olguin, J. Ho, X. L. Fan, C. Luo, C. S. Wang, K. Xu, *Science* **2015**, *350*, 938; b) X. L. Fan, L. Chen, O. Borodin, X. Ji, J. Chen, S. Hou, T. Deng, J. Zheng, C. Y. Yang, S. C. Liou, K. Amine, K. Xu, C. S. Wang, *Nat. Nanotechnol.* **2018**, *13*, 715; c) W. Xue, Z. Shi, M. Huang, S. Feng, C. Wang, F. Wang, J. Lopez, B. Qiao, G. Xu, W. Zhang, Y. Dong, R. Gao, Y. Shao-Horn, J. A. Johnson, J. Li, *Energy Environ. Sci.* **2020**, *13*, 212.
[79] L. Chen, J. Zhang, Q. Li, J. Vatamanu, X. Ji, T. P. Pollard, C. Cui, S. Hou, J. Chen, C. Yang, L. Ma, M. S. Ding, M. Garaga, S. Greenbaum, H.-S. Lee, O. Borodin, K. Xu, C. Wang, *ACS Energy Lett.* **2020**, *5*, 968.
[80] L. M. Suo, W. J. Xue, M. Gobet, S. G. Greenbaum, C. Wang, Y. M. Chen, W. L. Yang, Y. X. Li, J. Li, *Proc. Natl. Acad. Sci. USA* **2018**, *115*, 1156.
[81] a) L. B. Hu, Z. C. Zhang, K. Amine, *Electrochem. Commun.* **2013**, *35*, 76; b) X. Cao, X. He, J. Wang, H. D. Liu, S. Roser, B. R. Rad, M. Evertz, B. Streipert, J. Li, R. Wagner, M. Winter, I. Cekic-Laskovic, *ACS Appl. Mater. Interfaces* **2016**, *8*, 25971.
[82] a) Y. Uchimoto, K. Arnezawa, T. Furushita, M. Wakihara, I. Taniguchi, *Solid State Ionics* **2005**, *176*, 2377; b) M. Z. Liu,

© 2020 WILEY-VCH Verlag GmbH & Co. KGaA, Weinheim

B. Y. Jin, Q. H. Zhang, X. L. Zhan, F. Q. Chen, *J. Alloys Compd.* **2018**, *742*, 619; c) G. Homann, L. Stolz, J. Nair, I. C. Laskovic, M. Winter, J. Kasnatscheew, *Sci. Rep.* **2020**, *10*, 4390.

[83] J. H. Zhao, J. J. Zhang, P. Hu, J. Ma, X. G. Wang, L. P. Yue, G. J. Xu, B. S. Qin, Z. H. Liu, X. H. Zhou, G. L. Cui, *Electrochim. Acta* **2016**, *188*, 23.

[84] a) H. Kitaura, A. Hayashi, K. Tadanaga, M. Tatsumisago, *J. Electrochem. Soc.* **2010**, *157*, A407; b) H. Kitaura, A. Hayashi, K. Tadanaga, M. Tatsumisago, *Solid State Ionics* **2011**, *192*, 304; c) S. Yubuchi, Y. Ito, T. Matsuyama, A. Hayashi, M. Tatsumisago, *Solid State Ionics* **2016**, *285*, 79.

[85] G. Oh, M. Hirayama, O. Kwon, K. Suzuki, R. Kanno, *Chem. Mater.* **2016**, *28*, 2634.

[86] a) L. Miara, A. Windmuller, C. L. Tsai, W. D. Richards, Q. L. Ma, S. Uhlenbruck, O. Guillon, G. Ceder, *ACS Appl. Mater. Interfaces* **2016**, *8*, 26842; b) X. G. Liu, J. Tan, J. Fu, R. X. Yuan, H. Wen, C. H. Zhang, *ACS Appl. Mater. Interfaces* **2017**, *9*, 11696.

[87] a) J. B. Bates, G. R. Gruzalski, N. J. Dudney, C. F. Luck, X. H. Yu, *Solid State Ionics* **1994**, *70–71*, 619; b) M. Baba, N. Kumagai, N. Fujita, K. Ohta, K. Nishidate, S. Komaba, H. Groult, D. Devilliers, B. Kaplan, *J. Power Sources* **2001**, *97–98*, 798; c) J. Schwenzel, V. Thangadurai, W. Weppner, *J. Power Sources* **2006**, *154*, 232; d) C. Yada, A. Ohmori, K. Ide, H. Yamasaki, T. Kato, T. Saito, F. Sagane, Y. Iriyama, *Adv. Energy Mater.* **2014**, *4*, 1301416; e) J. C. Li, C. Ma, M. F. Chi, C. D. Liang, N. J. Dudney, *Adv. Energy Mater.* **2015**, *5*, 1401408; f) L. Li, S. Liu, H. Zhou, Q. Lei, K. Qian, *Mater. Lett.* **2018**, *216*, 135.

[88] S. Kim, M. Hirayama, K. Suzuki, R. Kanno, *Solid State Ionics* **2014**, *262*, 578.

[89] P. Y. Xu, W. Rheinheimer, S. N. Shuvo, Z. M. Qi, O. Levit, H. Y. Wang, Y. Ein-Eli, L. A. Stanciu, *ChemElectroChem* **2019**, *6*, 4576.

[90] Wikipedia, Spinel group, https://en.wikipedia.org/wiki/Spinel_group (accessed: February **2020**).

[91] A. Jain, S. P. Ong, G. Hautier, W. Chen, W. D. Richards, S. Dacek, S. Cholia, D. Gunter, D. Skinner, G. Ceder, K. A. Persson, *APL Mater.* **2013**, *1*, 011002.

[92] a) J. R. Dahn, E. W. Fuller, M. Obrovac, U. Vonsacken, *Solid State Ionics* **1994**, *69*, 265; b) R. Kanno, H. Kubo, Y. Kawamoto, T. Kamiyama, F. Izumi, Y. Takeda, M. Takano, *J. Solid State Chem.* **1994**, *110*, 216.

[93] D. Liu, W. Zhu, J. Trottier, C. Gagnon, F. Barray, A. Guerfi, A. Mauger, H. Groult, C. M. Julien, J. B. Goodenough, K. Zaghi, *RSC Adv.* **2014**, *4*, 154.

[94] W. D. Li, B. H. Song, A. Manthiram, *Chem. Soc. Rev.* **2017**, *46*, 3006.

[95] G. Hautier, A. Jain, S. P. Ong, B. Kang, C. Moore, R. Doe, G. Ceder, *Chem. Mater.* **2011**, *23*, 3495.

[96] J. Song, D. W. Shin, Y. H. Lu, C. D. Amos, A. Manthiram, J. B. Goodenough, *Chem. Mater.* **2012**, *24*, 3101.

[97] a) D. H. Seo, J. Lee, A. Urban, R. Malik, S. Kang, G. Ceder, *Nat. Chem.* **2016**, *8*, 692; b) G. Assat, J. M. Tarascon, *Nat. Energy* **2018**, *3*, 373.

[98] H. F. Wang, Y. I. Jang, B. Y. Huang, D. R. Sadoway, Y. T. Chiang, *J. Electrochem. Soc.* **1999**, *146*, 473.

[99] R. Yazami, Y. Ozawa, H. Gabrisch, B. Fultz, *Electrochim. Acta* **2004**, *50*, 385.

[100] J. Kikkawa, S. Terada, A. Gunji, T. Nagai, K. Kurashima, K. Kimoto, *J. Phys. Chem. C* **2015**, *119*, 15823.

[101] H. Y. Tan, S. Takeuchi, K. K. Bharathi, I. Takeuchi, L. A. Bendersky, *ACS Appl. Mater. Interfaces* **2016**, *8*, 6727.

[102] A. Yano, M. Shikano, A. Ueda, H. Sakaebe, Z. Ogumi, *J. Electrochem. Soc.* **2017**, *164*, A6116.

[103] W. M. Seong, K. Yoon, M. H. Lee, S. K. Jung, K. Kang, *Nano Lett.* **2019**, *19*, 29.

[104] K. W. Nam, S. M. Bak, E. Y. Hu, X. Q. Yu, Y. N. Zhou, X. J. Wang, L. J. Wu, Y. M. Zhu, K. Y. Chung, X. Q. Yang, *Adv. Funct. Mater.* **2013**, *23*, 1047.

[105] S. K. Jung, H. Gwon, J. Hong, K. Y. Park, D. H. Seo, H. Kim, J. Hyun, W. Yang, K. Kang, *Adv. Energy Mater.* **2014**, *4*, 1300787.

[106] F. Lin, I. M. Markus, D. Nordlund, T. C. Weng, M. D. Asta, H. L. L. Xin, M. M. Doeff, *Nat. Commun.* **2014**, *5*, 3529.

[107] H. Kim, M. G. Kim, H. Y. Jeong, H. Nam, J. Cho, *Nano Lett.* **2015**, *15*, 2111.

[108] J. Hong, D. H. Seo, S. W. Kim, H. Gwon, S. T. Oh, K. Kang, *J. Mater. Chem.* **2010**, *20*, 10179.

[109] A. Ito, K. Shoda, Y. Sato, M. Hatano, H. Horie, Y. Ohsawa, *J. Power Sources* **2011**, *196*, 4785.

[110] B. Xu, C. R. Fell, M. F. Chi, Y. S. Meng, *Energy Environ. Sci.* **2011**, *4*, 2223.

[111] M. Gu, I. Belharouak, J. M. Zheng, H. M. Wu, J. Xiao, A. Genc, K. Amine, S. Thevuthasan, D. R. Baer, J. G. Zhang, N. D. Browning, J. Liu, C. M. Wang, *ACS Nano* **2013**, *7*, 760.

[112] J. M. Zheng, P. H. Xu, M. Gu, J. Xiao, N. D. Browning, P. F. Yan, C. M. Wang, J. G. Zhang, *Chem. Mater.* **2015**, *27*, 1381.

[113] P. F. Yan, A. M. Nie, J. M. Zheng, Y. G. Zhou, D. P. Lu, X. F. Zhang, R. Xu, I. Belharouak, X. T. Zu, J. Xiao, K. Amine, J. Liu, F. Gao, R. Shahbazian-Yassar, J. G. Zhang, C. M. Wang, *Nano Lett.* **2015**, *15*, 514.

[114] P. F. Yan, J. M. Zheng, Z. K. Tang, A. Devaraj, G. Y. Chen, K. Amine, J. G. Zhang, L. M. Liu, C. M. Wang, *Nat. Nanotechnol.* **2019**, *14*, 602.

[115] S. M. Bak, E. Y. Hu, Y. N. Zhou, X. Q. Yu, S. D. Senanayake, S. J. Cho, K. B. Kim, K. Y. Chung, X. Q. Yang, K. W. Nam, *ACS Appl. Mater. Interfaces* **2014**, *6*, 22594.

[116] a) S. H. Park, S. H. Kang, C. S. Johnson, K. Amine, M. M. Thackeray, *Electrochem. Commun.* **2007**, *9*, 262; b) J. R. Croy, J. S. Park, Y. Shin, B. T. Yonemoto, M. Balasubramanian, B. R. Long, Y. Ren, M. M. Thackeray, *J. Power Sources* **2016**, *334*, 213.

[117] a) Y. Cho, S. Lee, Y. Lee, T. Hong, J. Cho, *Adv. Energy Mater.* **2011**, *1*, 821; b) F. Wu, N. Li, Y. F. Su, L. J. Zhan, L. Y. Bao, J. Wang, L. Chen, Y. Zheng, L. Q. Dai, J. Y. Peng, S. Chen, *Nano Lett.* **2014**, *14*, 3550; c) J. H. Shim, K. S. Lee, A. Missyul, J. Lee, B. Linn, E. C. Lee, S. Lee, *Chem. Mater.* **2015**, *27*, 3273; d) P. Oh, B. H. Song, W. D. Li, A. Manthiram, *J. Mater. Chem. A* **2016**, *4*, 5839; e) X. D. Zhang, J. L. Shi, J. Y. Liang, Y. X. Yin, J. N. Zhang, X. Q. Yu, Y. G. Guo, *Adv. Mater.* **2018**, *30*, 1801751.

[118] Z. Q. Rong, R. Malik, P. Canepa, G. S. Gautam, M. Liu, A. Jain, K. Persson, G. Ceder, *Chem. Mater.* **2015**, *27*, 6016.

[119] a) B. J. Johnson, D. H. Doughty, J. A. Voigt, T. J. Boyle, *J. Power Sources* **1997**, *68*, 634; b) M. Y. Saidi, J. Barker, R. Koksbang, *J. Solid State Chem.* **1996**, *122*, 195; c) M. Wakihara, G. H. Li, H. Ikuta, T. Uchida, *Solid State Ionics* **1996**, *86–88*, 907; d) F. Cao, J. Prakash, *Electrochim. Acta* **2002**, *47*, 1607; e) H. J. Bang, V. S. Donepudi, J. Prakash, *Electrochim. Acta* **2002**, *48*, 443; f) A. Ito, D. Li, Y. Lee, K. Kobayakawa, Y. Sato, *J. Power Sources* **2008**, *185*, 1429; g) A. Veluchamy, H. Ikuta, M. Wakihara, *Solid State Ionics* **2001**, *143*, 161; h) K. M. Shaju, G. V. S. Rao, B. V. R. Chowdari, *J. Mater. Chem.* **2003**, *13*, 106; i) D. Kovacheva, B. Markovsky, G. Salitra, Y. Talyosef, M. Gorova, E. Levi, M. Riboch, H. J. Kim, D. Aurbach, *Electrochim. Acta* **2005**, *50*, 5553; j) H. Xia, Y. S. Meng, L. Lu, G. Ceder, *J. Electrochem. Soc.* **2007**, *154*, A737; k) M. Park, X. C. Zhang, M. D. Chung, G. B. Less, A. M. Sastry, *J. Power Sources* **2010**, *195*, 7904; l) R. Amin, I. Belharouak, *J. Power Sources* **2017**, *348*, 318.

[120] X. H. Ma, B. Kang, G. Ceder, *J. Electrochem. Soc.* **2010**, *157*, A925.

[121] M. J. Lee, E. Lho, P. Bai, S. Chae, J. Li, J. Cho, *Nano Lett.* **2017**, *17*, 3744.

[122] a) T. Yuan, Z. P. Tan, C. R. Ma, J. H. Yang, Z. F. Ma, S. Y. Zheng, *Adv. Energy Mater.* **2017**, *7*, 1601625; b) S. T. Wang, Y. Yang, Y. H. Dong, Z. T. Zhang, Z. L. Tang, *J. Adv. Ceram.* **2019**, *8*, 1.

[123] S. T. Wang, W. Quan, Z. Zhu, Y. Yang, Q. Liu, Y. Ren, X. Y. Zhang, R. Xu, Y. Hong, Z. T. Zhang, K. Amine, Z. L. Tang, J. Lu, J. Li, *Nat. Commun.* **2017**, *8*, 627.

[124] W. Zhang, D. H. Seo, T. Chen, L. J. Wu, M. Topsakal, Y. M. Zhu, D. Y. Lu, G. Ceder, F. Wang, *Science* **2020**, *367*, 1030.

[125] A. Urban, J. Lee, G. Ceder, *Adv. Energy Mater.* **2014**, *4*, 1400478.

[126] J. Lee, D. A. Kitchaev, D. H. Kwon, C. W. Lee, J. K. Papp, Y. S. Liu, Z. Y. Lun, R. J. Clement, T. Shi, B. D. McCloskey, J. H. Guo, M. Balasubramanian, G. Ceder, *Nature* **2018**, *556*, 185.

© 2020 WILEY-VCH Verlag GmbH & Co. KGaA, Weinheim